Theory of reactions between hydrogen and group-III acceptors in silicon

José Coutinho[®], ¹ Diana Gomes[®], ¹ Vitor J. B. Torres[®], ¹ Tarek O. Abdul Fattah[®], ² Vladimir P. Markevich[®], ² and Anthony R. Peaker[®]

¹13N, Department of Physics, University of Aveiro, Campus Santiago, 3810-193 Aveiro, Portugal*

²Photon Science Institute and Department of Electrical and Electronic Engineering,

The University of Manchester, Manchester M13 9PL, United Kingdom

The thermodynamics of several reactions involving atomic and molecular hydrogen with group-III acceptors is investigated. The results provide a first-principles-level account of thermally- and carrier-activated processes involving these species. Acceptor-hydrogen pairing is revisited as well. We present a refined physicochemical picture of long-range migration, compensation effects, and short-range reactions, leading to fully passivated $\equiv \text{Si-H}\cdots X \equiv \text{structures}$, where X is a group-III acceptor element. The formation and dissociation of acceptor-H and acceptor-H₂ complexes is considered in the context of Light and elevated Temperature Induced Degradation (LeTID) of silicon-based solar cells. Besides explaining observed trends and answering several fundamental questions regarding the properties of acceptor-hydrogen pairing, we find that the BH₂ complex is a by-product along the reaction of H₂ molecules with boron toward the formation of BH pairs (along with subtraction of free holes). The calculated changes in Helmholtz free energies upon the considered defect reactions, as well as activation barriers for BH₂ formation/dissociation (close to \sim 1 eV) are compatible with the experimentally determined activation energies of degradation/recovery rates of Si:B-based cells during LeTID. Dihydrogenated acceptors heavier than boron are anticipated to be effective-mass-like shallow donors, and therefore, unlikely to show similar non-radiative recombination activity.

Pre-print published in Physical Review B 108, 014111 (2023)

DOI:10.1103/PhysRevB.108.014111

I. INTRODUCTION

Among all impurities studied in crystalline silicon, hydrogen has attracted much attention, if not the most [1–5]. Isolated atomic hydrogen in Si shows amphoteric character, high mobility as well as the ability to form strong bonds with other elements. This combination of properties has made H especially useful in many bulk [6–8] and surface [9–11] engineering processes, with profound impact on device performance.

The generally accepted picture of isolated H in Si is that of a species that can trap a hole to become a proton located at the center of a Si-Si bond. However, it can also trap an electron to form a H⁻ ion, which according to theorists, finds its most stable state at (or close to) the tetrahedral interstitial site [12–17]. The bistability of H is at the origin of the negative-U of its neutral state, which disproportionates into ionic species, $H^0 \rightarrow xH^+ + (1-x)H^-$, with the fractional concentration x depending on the location of the Fermi level with respect to the (-/+) transition level [13], estimated experimentally in the range 0.3-0.4 eV below the conduction band bottom [18–20].

Hydrogen-related defect engineering has conspicuous applications in the solar industry. Generally, Si solar cells feature a hydrogen-rich silicon nitride (SiN_x :H) or oxide layers deposited over the surface, providing chemical passivation, external anti-reflection to sunlight, as well as a highly-reflective interface to maximize the length of internal light paths. After SiN_x :H deposition, a step known as *fast-firing* (essentially a 750-850 °C annealing for a few seconds), induces the injection of substantial quantities of hydrogen from

the passivating layer into the silicon [21, 22], improving the quality of the interface, and further suppressing bulk and surface recombination events.

The presence of H in Si is also crucial for preventing the boron-oxygen-related light-induced degradation (BO-LID) of Si solar cells [23–25]. BO-LID is related to a decrease of minority carrier lifetime of cells based on B-doped O-rich silicon upon exposure to sunlight in a time scale of hours [26, 27]. It has been found that Si:(B+O)-based devices that were fired and subsequently annealed with illumination or with minority carrier injection (a process originally referred to as regeneration [23]), do not suffer from BO-LID. An examination of the BO-LID and regeneration kinetics in boron-doped p-type Czochralski-grown wafers, shows a clear dependence on the hydrogen content with a linear increase of the regeneration rate constant with increasing the bulk hydrogen concentration [25]. Regeneration of solar Si was recently proposed to result from H-passivation of the boron-dioxygen complex (BO₂) due to relocation of H from dissociated boron-hydrogen (BH) pairs [28]. Although it is generally thought that light can act as a catalyst for BH dissociation, it is not clear how that works.

Hydrogen in silicon has been found to be responsible for detrimental effects as well. Perhaps the most paradigmatic is the passivation of dopants upon H-acceptor and H-donor pair formation [6, 29–32]. Hydrogen-related reactions seem to be intimately related to yet another lifetime degradation effect. This is known as Light- and elevated-Temperature-Induced Degradation (LeTID) of solar Si [33]. Accordingly, photovoltaic modules show a substantial decrease of conversion efficiency (up to 16% relative) due to carrier lifetime shortening, and for that reason, it is currently an active topic of research. The LeTID designation was originally coined as to reflect the fact that light exposure and heat are needed for its observation, but the presence of hydrogen was subsequently

^{*} jose.coutinho@ua.pt

deemed necessary as well [34]. Typically, the effect is manifested as a drop of the carrier lifetime upon field-prolonged operation (time-scale of years) of solar cells followed by a recovery. However, accelerated lab conditions, either subjecting the cells to $\sim 100~^{\circ}\text{C}$ anneals with $\sim 1~\text{kW/m}^2$ (one sun) of illumination which is mostly above band gap, or passing a current to inject minority carriers equivalent to the population produced during normal operation, result in a maximum drop of the lifetime within hours. The latter procedure is nowadays almost universally used for LeTID testing, and for that reason, sometimes the effect is referred to as *carrier induced degradation*.

Dark anneals were also found to reproduce the LeTID effect, although at a considerably slower rate than with illumination, allowing for discrimination of LeTID from BO-LID. At $T=140\,^{\circ}$ C, maximum degradation was attained after more than 100 hours [35]. From this work, activation energies of 1.08 eV for degradation and 1.11 eV for recovery were measured during prolonged dark-annealing treatments. Importantly, and despite having been observed in several materials (multi-crystalline, Czochralski and floating-zone grown, p- and n-type), the firing step was found to be an indispensable ingredient for LeTID. This led to the conclusion that hydrogen is a constituent or somehow involved in the formation of the defect responsible for the non-radiative recombination of photogenerated carriers (see Ref. [36] for a review of LeTID of Si solar cells).

During the high-temperature firing step, the hydrogen introduced into the Si is only stable in the form of ions, which become distributed across the whole thickness of the wafers [22]. However, after cooling to room temperature, most of the hydrogen in the Si bulk forms H₂ molecules, either isolated or trapped next to impurities or defects [37, 38]. This is the usual state of hydrogen in *as-fired* (pre-degraded) cells.

Isolated H_2 molecules in crystalline Si start to migrate just above 300 K. However, in O-rich material they are weakly bound to interstitial O atoms (with a binding energy of 0.28 eV), so that one needs to raise the temperature up to around 70 °C to initiate molecular motion [39]. Upon annealing boron-doped Si above 160 °C, the molecules are known to interact effectively with boron atoms and form BH pairs. This reaction has been monitored either by local vibrational mode (LVM) infra-red absorption spectroscopy [38, 40] or by changes in resistivity [41, 42].

Recently, several groups have been investigating possible correlations between the LeTID degradation and the evolution of hydrogen, most notably in boron-doped Si, by monitoring the formation/dissociation of BH pairs [43–47].

Upon subjecting as-fired samples to isochronal annealings at several temperatures, Fung *et al.* [43] found that the maximum LeTID defect density correlated with the BO-LID regeneration rate (recently suggested to reflect the formation of a BO₂-H complex [28]), as well as with formation of BH pairs. Similar observations were reported by Hammann *et al.* [46, 48] who found a correlation between the LeTID defect formation kinetics and changes in resistivity, assumed to be due to BH formation, with both quantities reaching their maximum values at around the same time.

Winter *et al.* [44] used the three-state-model of Voronkov and Falster [41],

$$H_{2A} + 2B^- + 2h^+ \rightleftharpoons 2HB \rightleftharpoons H_{2C} + 2B^- + 2h^+, \quad (1)$$

to describe the dynamics of free-hole concentration (decrease followed by recovery) in floating-zone Si subject to surface passivation/firing and dark annealings. In the above model, H_{2A} and H_{2C} stand for two different types of H-dimers. The first refers to molecular hydrogen at tetrahedral interstitial sites of the Si lattice [37, 38]. The second dimer, although unidentified, must be a more stable state than that of the molecules [41]. It should be noted that according to the model presented in Ref. [41], the first step (left-side) of reaction 1 initiates with the dissociation of H_{2A} upon its interaction with a hole. The resulting positively charged H atoms then interact effectively with negatively charged B atoms to form BH pairs. From the experimental data it was possible to extract activation energies for formation and dissociation of the BH pairs as 1.29±0.07 eV and 1.22±0.18 eV [44], respectively. These figures were attributed to the rate-limiting processes of first (left-side) and second (right-side) steps of reaction 1 toward the right direction.

More recently, from prolonged dark annealings of SiN_x :H-coated/fired structures, Walter and co-workers [45] found respectively transient and equilibrium activation energies of 0.84 ± 0.17 eV and 1.35 ± 0.15 eV for the first step of reaction 1. The first quantity refers to the same property that was reported in Ref. [44] as being 1.29 ± 0.07 eV. A third measurement of this quantity was carried out by Acker *et al.* [49] and gave 1.20 ± 0.02 eV. This point needs clarification, not only because the values derived differ by more than their error bars added together, but also because they are close to 1.08 ± 0.05 eV that was measured by Vargas and co-workers [35] for the activation energy of the LeTID kinetics under 160 °C prolonged dark anneals.

It is highly desirable to understand what happens if we change the acceptor species. Are other group-III impurities able to interact with $\rm H_2$ molecules? Could the molecule dissociate upon reaction with the acceptors? What are the consequences to the LeTID effect? According to Ref. [49], GaH pairs were effectively formed in gallium-doped floating-zone Si structures that were annealed in the dark. From Arrhenius plots, an activation energy of 1.04 ± 0.01 eV was extracted for the growth rate of the GaH pair concentration, suggesting a faster $\rm H_2$ dissociation upon reaction with Ga than B.

Grant *et al.* [50] compared LeTID of B- and Ga-based cells, the former being subject to a regeneration treatment (see above) at the last stage of fabrication. They found that under 1 sun illumination at 75 °C, the B-based cells remained stable, whereas Ga-doped devices showed a slight degradation. It was however found that 30-min dark anneals in the range 200-300 °C resulted in suppression of the stabilizing effect of the regeneration treatment, leading to strong LeTID in the B-doped cells. The extent of LeTID in Ga-doped cells also increased after the 200-300 °C anneals.

According to Ref. [51], the degradation rate in Ga-doped cells was different to what is usually observed in B-based de-

vices. In the Ga-doped structures, whereas almost no degradation occurred under 1 sun illumination at 75 °C, a lifetime decrease was found upon exposure to low light intensity. It was suggested that the dopant species plays an active role in the reactions governing LeTID, possibly involving differences in the properties of the respective acceptor-hydrogen pairs.

Regarding the atomistic and electronic structure of the BH pairs, the common view is that they form a three-center B-H-Si structure, where H sits at the bond center site between B and its Si first neighbor. The pairs are understood to be electrically inert, although during the early stages of research in this field, intense discussions took place on whether their neutralization was due to compensation or passivation [31, 52–56]. In the first case, hole transfer takes place from B to H, driving the formation of close B⁻H⁺ ionic pairs. In the second case, H is covalently bound to Si, leaving B three-fold coordinated and both B and H atoms are neutral. Experiments favor the latter view, and it is now generally accepted that the hydrogen truly passivates the acceptor.

Multiple H trapping by boron was also anticipated earlier [57, 58]. Based on junction capacitance measurements and first-principles calculations, we recently proposed that a boron-dihydrogen complex, possessing a donor level at 0.175 eV below the conduction band bottom, and showing a large capture cross-section for electrons, could be responsible for LeTID behavior based on boron-doped Si materials [59]. This proposal raises many questions, starting with the formation/activation and destruction/inhibition mechanisms of such complexes. And what about dihydrogenation of other acceptors species? What are the properties of the corresponding complexes?

Besides the above, additional fundamental questions regarding the interaction of H with p-type dopants, have been left unanswered for decades. These need to be addressed as well. We refer for instance, to the unexpected trend observed for the dissociation energies of XH pairs (X being one of B, Al, Ga and In), which do not show a monotonic variation with the acceptor atomic number [60]. Also surprisingly, BH shows the lowest dissociation energy (compared to other XH pairs). Being the smallest atom among the group-III acceptors, boron is expected to allow for relatively more room to accommodate H within the X-H-Si structure, and therefore to show the largest binding energy to H.

Another puzzle worthy of mention is the observation of a splitting pattern for the BH-related vibrational peak, measured by Raman spectroscopy and positioned at $1903~\rm cm^{-1}$ under uniaxial stress along the $\langle 100 \rangle$ direction [61]. Based on the premise that this mode involves the stretching of a Si-H bond, it was concluded that the B-H-Si structure could not be linear, and the symmetry of the BH pair could not be trigonal. Instead, it was proposed that the H atom should be located at an "off-bond-centered" site [61]. However, this clashes with the generality of the theoretical results, where trigonal symmetry was found [31, 56, 59, 62–64].

This work aims at providing a modern view of the solidstate physics of acceptor-hydrogen interactions in p-type silicon. Effects of temperature and the presence of minority carriers were given special attention. Besides shedding light on the open issues identified above, we have investigated the thermodynamics of the most probable solid-state reactions involving hydrogen and group-III acceptors. Other competing reactions involving hydrogen interaction with two of the most abundant impurities in Si materials, namely oxygen and carbon, are also investigated.

We start by describing the methodologies in Sec. II. In Sec. III A we analyze the acceptor-hydrogen bonding chemistry, its relation to the passivation effect, as well as the dynamics of H in the vicinity of the acceptors. In Sec. III B we explore the formation and dissociation mechanism of acceptor-H pairs in Si. Chemical trends, temperature and carrier trapping effects are discussed. In Sec. III C we report on the interactions of H₂ molecules with oxygen, carbon and group-III acceptors in Si. Strain induced interactions, formation of remote and closely spaced impurity-H₂ pairs, as well as properties of the complexes resulting from intimate chemical reactions (which lead to changes in the bonding properties of the reactants) are described. The temperature-dependent energy balance of these reactions is also reported at this stage. In Sec. III D we look at the local vibrational mode (LVM) frequencies of boronhydrogen complexes in Si. Here we describe a comparative study, with the results being examined in the light of experimentally well characterized frequencies from elemental boron and hydrogen defects. We end the paper in Sec. IV, where we discuss our findings and the conclusions are drawn.

II. THEORETICAL METHODS

A. Semi-local and non-local all-electron energies

First-principles calculations were carried out using the density functional Vienna Ab-initio Simulation Package (VASP) [65–67], employing the projector-augmented wave (PAW) method for the treatment of electronic core states [68]. A basis set of plane-waves with kinetic energy of up to 400 eV was used to describe the Kohn-Sham states. Total energies were evaluated self-consistently, using the hybrid density functional of Heyd-Scuseria-Ernzerhof (HSE06) [69, 70] with a numerical accuracy of 10^{-6} eV. When compared to generalized gradient approximated (GGA) calculations [71], which underestimate the band gap of Si by nearly 50%, the HSE06 functional gives a band gap of 1.1 eV for Si. This is about the figure measured experimentally, allowing us to obtain first-principles ~ 0.1 eV-accurate electronic transitions between gap states and the band edges.

Defect energies were found using 512-atom (defect-free) supercells of Si, obtained by replication of $4\times4\times4$ conventional unit cells (lattice constant $a_0=5.4318$ Å). Defect structures were firstly optimized within the GGA approximation [71] using $\mathbf{k}=\Gamma$ to sample the Brillouin zone (BZ), until the largest force became lower than 0.01 eV/Å. Tests on selected defects using a finer sampling (Γ -centered grid of $2\times2\times2$ points) were carried out in order to verify the quality of the forces and structures. The total energies (electronic and ionic) of defects were found from single-point HSE06-level calculations of the GGA-level structures (keeping the band structure

sampled at $\mathbf{k} = \Gamma$).

B. Defect properties

Transition energy levels of defects, E(q/q'), quantify the location of the Fermi level above/below which a defect is more stable in q/q' charge state, respectively. These were evaluated with respect to the valence band top (E_v) according to the usual methodology (see for example Ref. [72] and references therein),

$$E(q/q') - E_{\rm v} = -\frac{E(q) - E(q')}{q - q'} - E_{\rm v}^{\rm KS},$$
 (2)

where E(q) is the total energy of the defect, and $E_{\rm v}^{\rm KS}$ is the calculated valence band top (highest occupied Kohn-Sham state at $\mathbf{k} = \Gamma$ of a 512-atom bulk supercell).

For non-zero charge states, the energies in Eq. 2 are subject to a correction, $E(q) = \tilde{E}(q) + E_{\rm corr}(q)$. This aims at removing the spurious electrostatic interactions between the artificial lattice of charges and neutralizing background that are implicitly created in periodic calculations [73]. Here $\tilde{E}(q)$ is the total energy as found for the periodic system, while E(q) is now the (approximate) energy of the aperiodic problem. For a localized defect, $E_{\rm corr}$ scales as q^2/L , where L is a characteristic length of the supercell. In the present case we investigated single donors/acceptors $(q=\pm 1)$ and the corrections were smaller than 0.1 eV.

It is known that periodic charge corrections tend to work better when the charge trapped at the defect is well contained within the supercell [74]. Some of the defects studied are shallow acceptors, and for those we used an empirical approach, much in the spirit of the marker method of Resende *et al.* [75]. This method relies on error cancellation and usually leads to sub-0.1 eV error bars [76]. Accordingly, $E_{\text{corr},X}(-1)$ for a shallow acceptor complex incorporating a group-III species X, is obtained from the error of the calculated hole binding energy for the respective isolated acceptor,

$$E_{\text{corr},X}(-1) = E_{\text{h},X}^{\text{exp}} - \left[\tilde{E}_X(-1) - \tilde{E}_X(0) - E_{\text{v}}^{\text{KS}}\right]$$
 (3)

where $E_{\mathrm{h},X}^{\mathrm{exp}}=46,72,74,157$ meV are measured hole binding energies, for $X=\mathrm{B}$, Al, Ga, and In shallow acceptors in silicon, respectively [77], and \tilde{E}_X are (uncorrected) energies of supercells with the appropriate substitutional acceptor. Values of $E_{\mathrm{corr},X}$ were between -20 and -13 meV.

Vibrational modes and their frequencies were obtained within the harmonic approximation using density functional perturbation theory (DFPT) [78]. This method gives analytical access to the dynamical matrix elements from the gradient of the electron density relative to atomic displacement and, from here, to the vibrational properties without having to displace the atoms explicitly. These calculations were performed within the GGA-level, on supercells with 64 atoms, a Brillouin zone sampling grid of $2 \times 2 \times 2$ special **k**-points, using $E_{\text{cut}} = 500$ eV, and the relaxed structures had residual

forces below 0.005 eV/Å. Besides the calculation of local vibrational modes, resonant mode frequencies were also found for the calculation of vibrational free energies (see below).

The intensity of IR absorption bands associated with a LVM was estimated from its oscillator strength [79, 80],

$$f(m) = \sum_{i} \sum_{\alpha,j} \left| Z_{\alpha,ij}^* e_{\alpha,j}(m) \right|^2 \tag{4}$$

where the summation runs over all atoms with index α , as well as Cartesian coordinate indexes i and j. The calculation of the Born effective charge tensor for each atom, $Z_{\alpha,ij}^* = V \partial P_i / \partial R_{\alpha,j}$, involves finding the macroscopic polarization (**P**) of a defective supercell with volume V, and its response to atomic displacements (**R**). In practice this is done using a finite difference method. The polarization was conveniently found within DFPT (see Sec. II.D.2 of Ref. [78] and Ref. [81] for an implementation of the PAW method). Finally, the quantity $e_{\alpha,j}(m)$ is the m-th mode mass-weighted eigenvector.

The elastic coupling of defects to the lattice can be described by the elastic dipole tensor (P_{ij}) . Accordingly, the elastic energy of a defective supercell subject to external homogeneous strain field ε_{ij} is [82, 83],

$$E = V c_{ijkl} \varepsilon_{ij} \varepsilon_{kl} - P_{ij} \varepsilon_{ij}, \tag{5}$$

where c_{ijkl} are the elastic constants of the material. Minimization of Eq. 5 with respect to strain leads to

$$P_{ij} = V c_{ijkl} \varepsilon_{kl} = -V \sigma_{ij}. \tag{6}$$

The first equality allows us to find the dipole tensor from the strain ε_{kl} produced by a defect in a fully relaxed supercell with optimized lattice vectors and atomic geometry. From the second equality on the other hand, P_{ij} can be obtained from the stress σ_{ij} developed across the supercell, whose volume V and shape are kept invariant upon relaxation of the atomistic structure. The second approach is usually more practical, and it was the one used by us.

The elastic dipole tensor is related to another useful quantity, namely the relaxation volume tensor, $\Omega_{ij} = s_{ijkl}P_{kl}$, whose trace is related to the elastic relaxation volume of the defect, $\Omega_{\rm rel} = {\rm Tr}\Omega$, where s_{ijkl} are the elastic compliance tensor elements of the crystal [82, 83]. The relaxation volume quantifies the macroscopic volume change of a sample upon defect introduction.

The bonding character of hydrogen to the dopants was investigated using the Electron Localization Function (ELF) as defined by Becke and Edgecombe [84], and later explored for bond topology analysis by Silvi and Savin [85]. Accordingly,

$$ELF(\mathbf{r}) = \frac{1}{1 + \chi^2(\mathbf{r})},\tag{7}$$

where $\chi = D_P/D_h$ is the ratio of the kinetic energy density due to Pauli repulsion between electron pairs to the kinetic energy density of the homogeneous electron gas,

$$D_{\mathbf{P}}(\mathbf{r}) = \frac{1}{2} \sum_{i=\text{occ}} |\nabla \psi_i(\mathbf{r})|^2 - \frac{1}{8} \frac{|\nabla n(\mathbf{r})|^2}{n(\mathbf{r})}, \tag{8}$$

$$D_{\rm h}(\mathbf{r}) = \frac{3}{10} \left(3\pi^2 n(\mathbf{r}) \right)^{5/3}. \tag{9}$$

The second term in Eq. 8 is the Boson-like kinetic energy density of electrons [84], which is subtracted to the Fermionic kinetic energy density (first term), so that $D_{\rm P}$ becomes the contribution from Pauli repulsion effects alone. The electron density n is obtained from contributions of all occupied Kohn-Sham orbitals, $n = \sum_{i={\rm occ}} |\psi_i|^2$. $D_{\rm P}$ is therefore a positive definite quantity (the local Fermionic kinetic energy is always greater than the Bosonic counterpart), and approaches zero when electrons are alone or form pairs of opposite spins, i.e., when they are Boson-like. Hence, ELF provides a quantitative method for mapping the localization of bonds and radicals.

The ELF is a scalar field with $0 \le \text{ELF} \le 1$, where 1 corresponds to a perfect localization either of a pair of opposite spins (like in a covalent bond or a lone pair), or to an unpaired electron (like in a radical). These correspond to maxima of ELF and are referred to as *attractors*. Values of ELF are small in the border that separates highly localized regions, and ELF = 1/2 when the electron density corresponds to that of the homogeneous electron gas, which enters in the normalization of χ and provides a physical reference. The ELF is represented graphically with help of isosurfaces at a specific cut-off ELF₀, such that each enclosed volume defines an ELF shell associated with a single attractor.

C. Reaction barriers and free energies

We have estimated the Helmholtz free energy of defect reactions. Besides the (zero-temperature) potential energy change, this quantity describes the change of electronic and ionic degrees of freedom between reactants and products at finite temperatures, including the change in configurational entropy ($\Delta F = \Delta F_{\rm elec} + \Delta F_{\rm ion} - T\Delta S_{\rm conf}$). The frozen core approximation of the pseudopotentials implies that $\Delta F_{\rm elec}$ accounts for the valence electrons (electron-electron and electron-ion interactions), while analogous interactions involving core electrons are accounted for by $\Delta F_{\rm ion}$.

In many cases, we deal with electrically neutral defects or deep carrier traps, for which the electronic entropy change vanishes or it is negligible up to several hundred degrees Kelvin [86]. Accordingly, we assumed that $\Delta F_{\rm elec} = \Delta E_{\rm elec}$, which is the static all-electron potential energy change. The ionic free energy, $\Delta F_{\rm ion} = \Delta E_{\rm ion} + \Delta F_{\rm vib} + \Delta F_{\rm rot}$ accounts for the static ionic potential energy, as well as vibrational and rotational free energies. For practical reasons, we reorganize the above terms as

$$\Delta F = \Delta E + \Delta F_{\text{vib}} + \Delta F_{\text{rot}} - T \Delta S_{\text{conf}}, \tag{10}$$

where ΔE lumps together the stationary electronic and ionic potential energies, here obtained from the density functional pseudopotential calculations.

The Helmholtz free energy is calculated within the harmonic and dilute approximations. The first assumes that the vibrational free energy of reactants and products can be obtained from a set of 3N-3 independent harmonic oscillators with frequency ω_i ,

$$F_{\text{vib}} = k_{\text{B}}T \sum_{i=1}^{3N-3} \ln \left[2 \sinh \left(\frac{\hbar \omega_i}{2k_{\text{B}}T} \right) \right], \tag{11}$$

which already accounts for zero-point vibrational motion, where k_B is the Boltzmann constant and \hbar the reduced Plank constant. The vibrational frequencies were obtained within the method already described above. Regarding the dilute regime, it means that we ignore defect-defect interactions, notably in the calculation of configurational entropy.

The rotational free energy in Eq. 10 is required for reactions involving H_2 molecules. Isolated molecules at tetrahedral interstitial sites are virtually free to rotate around their center of mass [87]. The free energy from this degree of freedom is $\Delta F_{\rm rot} = -k_{\rm B}T \ln Z_{\rm rot}$, where the rotational partition function $Z_{\rm rot} = Z_{\rm g}^{\rm go}Z_{\rm p}^{\rm gp}$ accounts for independent populations of ortho (o) and para (p) spin-isomers of the molecules,

$$Z_{\{\text{o,p}\}} = \sum_{j=\{\text{odd, even}\}} (2j+1) \exp[-j(j+1)\theta_{\text{rot}}/T],$$
 (12)

with natural occurring fractions $g_0 = 3/4$ and $g_p = 1/4$. The index *j* runs over odd (even) integers for ortho (para) H₂, and the characteristic rotational temperature is $\theta_{\text{rot}} = 73 \text{ K}$ [86].

Some defects were found to be shallow acceptors, and for reactions involving those species, we have to add a term $\Delta F_{\rm elec,h}$ to Eq. 10, which accounts for the electronic free energy change due to thermal emission of holes across the reaction. We restrict our analysis to temperatures and carrier concentrations in the context of LeTID. Hence, the free energy change is assumed to simply reflect the change in free carrier concentration due to full ionization/passivation of the acceptors. Details for the estimation of $\Delta F_{\rm elec,h}$ and configurational entropy are provided in Appendixes A-D.

The above method has been successfully used for the study of thermodynamic properties of defects in crystals [88–90], including hydrogen complexes in silicon [86, 91]. In the latter case, it was found that anharmonic effects become sizable above $T\sim 400\text{-}600~\text{K}$, in which case the conclusions drawn must be considered as qualitative [91].

The potential energy barriers of reactions were investigated using the climbing image nudged elastic band method (NEB) [92]. These calculations were carried out using 64-atom supercells and Γ -centered $2\times2\times2$ grids for sampling the BZ. First, we started by setting up an array of up to 11 supercells linearly interpolated between the stable end-configurations. On a second step, a NEB relaxation was performed with forces calculated at the GGA level. In a final and third step, the previous (GGA-grade) structures were used to obtain the minimum

energy path (MEP) by performing single-point calculations at HSE06 level (keeping the $2 \times 2 \times 2$ BZ sampling grid).

D. Notation and conventions

Before proceeding to the results section, we write a few words about notation and conventions adopted. The reaction energy of a process $A \rightarrow B$ is evaluated as $\Delta E_R = E_B - E_A$ and the corresponding binding energy (if applicable) is given by $E_b = -\Delta E_R$. Accordingly, $E_b > 0$ for an exothermic reaction, where E_A and E_B are energies of states A (reactants) and B (products), respectively.

Acceptor species X=B, Al, Ga, and In, are by default, assumed to occupy a substitutional site. Neutral and negative states are respectively referred to as X^0 and X^- . Carbon and oxygen impurities are considered to occupy substitutional and interstitial (bond centered) sites, respectively, and are referred to simply as C and O defects. Should any ambiguity arise, they are identified with commonly used subscripts as X_s and X_i , respectively.

Depending on its charge state, interstitial hydrogen in Si can adopt different configurations [13, 31]. By default, we assume that isolated positive and negative species stand for a bond-centered proton and anti-bonding hydride ion, respectively. They are respectively represented by H⁺ and H⁻. The energy of the often considered tetrahedral interstitial H⁻ state was only 0.04 eV higher than the anti-bonding one. Such tiny difference suggests that H⁻ is delocalized over the tetrahedral cage and effectively shows an averaged tetrahedral symmetry. Neutral hydrogen is most stable at the bond center site, and that is what H⁰ stands for (see Ref. [91] and references therein for a recent review of atomic and dimerized H in Si). Subscripted H symbols like HAB and HBC (referring to the impurity located at anti-bonding and bond-centered sites) are avoided. This terminology is, however, necessary when addressing inequivalent H atoms in a complex (e.g. H₂* and some boron-dihydride complexes).

As already mentioned, hydrogen in Si can form dimers, with at least H_2^* and H_2 molecules having been identified experimentally. We will be referring to the molecules (located at the tetrahedral interstitial sites) simply as H_2 . Other H-related dimers, in particular boron and carbon dihydride complexes have specific labels, namely BH_2 and CH_2 , respectively.

III. RESULTS

A. On the nature of the acceptor-H bonding

In agreement with previous reports [31, 52, 56, 62–64], our results show that the H atom in XH pairs finds its most favorable location between the acceptor and one of its Si first neighbors, forming a three-atom X-H-Si structure. For the case of BH, the point group symmetry of the resulting geometry is trigonal ($C_{3\nu}$), whereas the pairs involving heavier acceptors show a bent X-H-Si unit, forming an angle $\theta = 137^{\circ}$, 150° ,

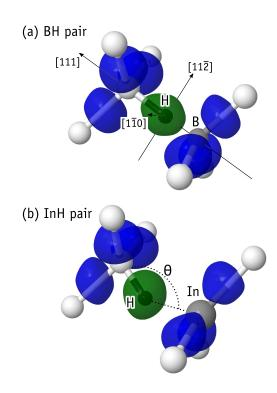


Figure 1. Isosurface of the valence electron localization function at ${\rm ELF}=0.8$ for (a) BH and (b) InH complexes in silicon. Blue surfaces represent ELF shells associated with Si-Si and Si-X bonds. Green surfaces represent protonated ELF shells associated with Si-H bonds. Silicon, hydrogen, and the acceptors are shown in white, black and gray, respectively. The In-H-Si angle and crystallographic directions are also indicated.

and 138° for AlH, GaH and InH, respectively. Equilibrium structures of BH and InH pairs are represented in Figure 1.

The nature of the local bonding of XH pairs was investigated with help of the ELF. Figs. 1(a) and 1(b) show ELF isosurfaces for BH and InH pairs, respectively, using a cut-off ELF = 0.8. We find two types of ELF shells associated with covalent bonds between pairs of atoms. The first kind are colored in blue and enclose ELF attractors that lie between a pair of atoms (Si-Si and Si-X bonds). Their localization is typical of covalent homopolar bonds. The second kind are protonated shells, clearly enclosing the H nuclei and displaced toward the nearest Si atom (see Figure 2 of Ref. [85] for details of bond classification using ELF). All shells were found to be populated with approximately 2 electrons. This result demonstrates a genuine passivation effect via formation of a Si-H covalent bond (not a compensation effect), and that the stable pairs should not be viewed as adjacent ionic X⁻H⁺ moieties. Instead, and as proposed by Pankove and co-workers [52], they are best described as fully saturated \equiv Si-H···X \equiv structures, where Si, X and H are four-fold, three-fold and mono coordinated, respectively. The three dots between H and X represent a steric interaction that depends on the size of the X species.

Of course, the calculated structure of BH is at variance with the one proposed by Herrero and Stutzmann [61], which resulted from interpretation of the stress splitting of the BH- related 1903 cm $^{-1}$ Raman peak under $\langle 100 \rangle$ uniaxial stress. We propose an alternative explanation, which reconciles the calculations with the stress experiments of Ref. [61] – the BH structure is trigonal, but the Raman peak at 1903 cm $^{-1}$ results from the coupling of the H-Si stretching mode with an undetected low-frequency doublet, possibly involving motion of H in the plane perpendicular to the symmetry axis. In that case, the measurements would reflect the splitting of the doublet under uniaxial stress.

The existence of a low-frequency degree of freedom coupled to the stretching mode in the *XH* pairs was actually postulated earlier by Stavola and co-workers [93, 94] in order to explain the observation of a pronounced red-shift of all acceptor-H stretching band frequencies (by more than 30 cm⁻¹) upon raising the temperature from liquid He up to room temperature [95]. Accordingly, with increasing the temperature, excited states of the low-frequency mode become increasingly populated, offsetting the transition energy related to the stretching mode by a few cm⁻¹. As noted in Ref. [93], the above picture is reminiscent of the vibrational spectra of interstitial oxygen, which also involves a stretching mode of a three-center Si-O-Si unit coupled to a two-dimensional low frequency mode of the order of 30 cm⁻¹, involving the motion of oxygen in the (111) plane [96–98].

We did not find a H-related wagging mode for BH above the Raman frequency of Si. We did actually find several low frequency modes in the range of 10-50 cm⁻¹ involving H motion in the (111) plane. However, because they are strongly mixed with the crystalline states, and the magnitude of their frequency is as low as the error bar of the calculations, all we can say is that (i) stress-splitting and temperature-dependent optical absorption experiments point to the existence of such a low frequency state, and that (ii) theory does not rule it out.

For XH complexes with heavier acceptors (showing off-bond-centered structures), a low frequency motion could involve the rotation of H around the bond center, leading to a roto-vibrational coupled model. Indeed, from the energies of relaxed $X\cdots H$ -Si structures with H displaced along [1 $\overline{10}$] and [11 $\overline{2}$], we estimate that the warping of the potential energy path for H rotation around the bond center site involves three equidistant barriers with height in the range 5-20 meV only. This is smaller than typical zero-point motion energies of H defects, suggesting that for the complexes with heavier X atoms (X = A1, Ga, In) the H atom is delocalized over a *donut* around the BC site, effectively showing trigonal symmetry like BH.

Another interesting observation against which XH models must be tested, involves the hopping of H between equivalent bond centered sites next to X. This was investigated by following the temperature-dependence of the recovery of the stress induced dichroism in the absorption spectra of samples where BH pairs were aligned under uniaxial stress [99]. From the data, a barrier of 0.19 eV was extracted. This figure was already reproduced theoretically as $E_a = 0.20$ eV by Denteneer *et al.* [31]. We found exactly the same value using the NEB method.

Analogous experiments were also reported for the InH pair using perturbed angular correlation spectroscopy to monitor

the anisotropy of hyperfine interactions of ¹¹¹In ions paired with H [100]. The stress was applied in situ, at room temperature, along $\langle 100 \rangle$, $\langle 110 \rangle$ and $\langle 111 \rangle$ directions, and with magnitude up to 0.2 GPa (about the same that was used for the alignment of BH in Ref. [99]). According to the authors, no preferential alignment of the InH pairs was observed. From a NEB calculation we found that the barrier for the jump of H between In-Si bonds amounts to $E_a = 0.71$ eV, i.e. considerably higher than that for H motion in BH. This could therefore explain the lack of a stress-induced alignment of the InH hyperfine signal at room temperature [100]. Such high barrier is attributed to the relatively large displacement of H in the transition state, which approaches the tetrahedral interstitial site next to In along $\langle 100 \rangle$. For the case of BH, the transition state consists of a relatively small BH dimer aligned along (100), sharing the substitutional site.

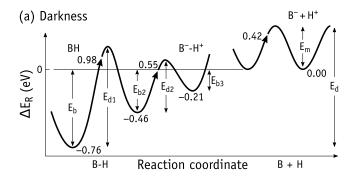
B. Formation and dissociation mechanisms of acceptor-H pairs

1. Binding energy of correlated acceptor-H pairs

We now look at the reaction $X^- + H^+ \to XH$. This is an important route for formation of XH in hydrogenated p-type Si. To find the binding energy of XH, the energy of the reactants was calculated using (charge-corrected) independent supercells. We also investigated the stability of close X^- - H^+ pairs, with H sitting on second and third neighboring bonds to X^- . A reaction coordinate diagram is shown in Fig. 2 for the specific case of BH formation, where the pairing reaction energy ΔE_R is represented as a function of the separation between B^- and H^+ . The zero energy corresponds to the state of fully independent reactants. We start by discussing BH formation/dissociation, and after that, we report the results and trends obtained for other acceptors.

The BH pair ground state has a calculated binding energy $E_{\rm b} = 0.76$ eV. This value nearly coincides with the experimental value of 0.75 eV obtained recently by Voronkov and Falster [41], and hopefully this clears some doubts regarding early calculations which found rather different figures, $E_b = 2.5 \text{ eV}$ [56] and $E_b = 0.59$ eV [31]. The first-neighboring BH pair is markedly more stable than second and third neighboring B-H pairs with $E_{b2} = 0.46$ eV and $E_{b3} = 0.21$ eV. To check for the existence (or not) of a capture barrier along the pairing reaction just before reaching the BH ground state structure, we calculated the potential energy surface for the hydrogen jump from first to second, and from second to third neighboring bond center sites with respect to boron. These calculations were performed using the NEB method spanning a total of 11 structure images along each path. As shown in Fig. 2(a), the "first dissociation" jump involves overcoming a barrier of nearly $E_{\rm d1}=1$ eV, whereas the barrier for a second jump (to the third neighboring bond center site) is only $E_{\rm d2} = 0.55 \, \rm eV$ high.

As H⁺ jumps further away from B⁻, the heights of the corresponding barriers are assumed to progressively decrease to-



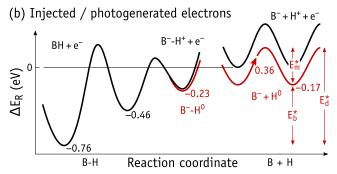


Figure 2. Configuration coordinate diagrams with reaction energies (ΔE_R) for boron-hydrogen pair formation in p-type silicon (a) under equilibrium dark conditions, and (b) in red, showing the effect of the presence of a free electron (e.g. due to current injection or photogeneration). Structures involving first neighboring pairs (BH), second and third neighboring pairs (B-H), and infinitely separated pairs (B+H) are considered. The calculated migration barrier of hydrogen (E_m) was taken from Ref. [91]. The zero energy reference corresponds to the $B^- + H^+$ state. Calculated figures for other dopants are reported in Table I.

ward the migration barrier of isolated $\mathrm{H^+}$. Using identical methodologies to those employed in this work, we recently reported the migration barrier of $\mathrm{H^+}$ in Si as $E_\mathrm{m}=0.42~\mathrm{eV}$ [91], implying that our estimate for the dissociation barrier of BH is $E_\mathrm{d}=1.18~\mathrm{eV}$. This figure is only 0.1 eV below the experimental result of Zundel and Weber [60]. Besides reassuring the validity of the formation/dissociation model presented above, this difference provides us with an estimate of the magnitude of the error bar for energy values of the order of 0.1 eV in our calculations.

Based on the calculated interactions between hydrogen and other group-III species in Si, we can carry out an analogous analysis regarding the formation and dissociation of XH pairs with X=Al, Ga, and In. The results are summarized in Table I for all species. The following aspects are worthy of note: (i) The calculated dissociation barriers (and binding energies) depend weakly on the acceptor species, $1.18\,\mathrm{eV} \le E_\mathrm{d} \le 1.37\,\mathrm{eV}$; (ii) BH shows a relatively smaller binding energy, and consequently a lower dissociation barrier; (iii) Among the three XH pairs with heavier acceptors, GaH shows a slightly smaller binding energy. All these features are also reflected in the measurements of Zundel and Weber [60] (c.f.) experimental dissociation barriers reproduced in Table I).

Table I. Binding energies (E_b) and dissociation energies (E_d) of acceptor-hydrogen (XH) pairs in silicon. Starred quantities refer to $XH + e^- \rightleftharpoons X^- + H^0$ reaction energies involving the capture/emission (rightward/leftward directions, respectively) of an electron by hydrogen at a remote location from the acceptor. See Figure 2 for a graphical description and definition of the energies. All values are in eV.

Acceptor	В	Al	Ga	In
$E_{\rm b}$	0.76	0.95	0.92	0.95
E_{b2}	0.46	0.32	0.34	0.28
E_{b3}	0.21	0.22	0.23	0.17
E_{b}^{*}	0.59	0.76	0.73	0.76
$E_{ m d}^*$	0.98	1.12	1.09	1.12
E_{d1}	0.98	0.74	0.74	0.67
$E_{\rm d}$	1.18	1.37	1.34	1.37
$E_{\rm d,exp}$ [60]	1.28	1.44	1.40	1.42

2. Unexpected dissociation energy trend

At least two obvious questions arise at this point. One of them is why the dissociation (and binding) energy of BH is distinctively smaller than the same quantity for the other pairs? After all, a small B atom is expected to share its site volume with H easier than larger acceptors are. The second question looks for an explanation for the non-monotonic trend in the observed and calculated dissociation energies, which show a small, unexpected decrease for GaH.

Let us first look at the issue pertaining to the small binding energy of BH. As we move downward along the group-III column of the periodic table, the increasing size of the acceptors lead to the buildup of compressive strain around the dopant. Calculated values of their relaxation volume $(\Omega_{\rm rel})$ are, respectively, $-20.6,\,1.6,\,1.4$ and $8.1\,\mbox{\normalfont\AA}^3$ for substitutional B $^-$, Al $^-$, Ga $^-$, and In $^-$. As described in Section III A, $\Omega_{\rm rel}$ quantifies the macroscopic volume change of a sample upon defect introduction. The results clearly reflect the tensile character of boron and the compressive nature of the remaining dopants. On the other hand, each isolated proton is estimated to add a volume $\Omega_{\rm rel}=13.5\,\mbox{\normalfont\AA}^3$ to the Si host.

From the above, we may expect a proton to be more stable in the middle of a B^- -Si bond than in between In^- and Si. We note however, that the binding energy of H^+ to X^- depends on the energy balance between both reactants and products, and additional arguments beyond the relaxation volume of the acceptors must be considered. For instance, while the B-H-Si structure is linear, other X-H-Si structures with larger acceptors are bent, and some of the strain working against the pairing is released.

Relaxation volumes of XH pairs are -6.3, 11.8, 11.8 and 18.6 Å³ for X = B, Al, Ga, and In, respectively. Considering the volumes of the isolated species reported above, we find that the whole relaxation volume change along the reaction $X^- + H^+ \to XH$ is $\Delta\Omega_R = 0.8, -3.2, -3.1$, and -3.0 Å³, indicating that after all, for the purpose of comparing the binding energies of different XH pairs, strain effects are not that

important.

On the other hand, from the perspective of the local chemical bonding, the reaction

$$X^-$$
-Si + Si-H⁺-Si $\rightleftharpoons X \cdots$ H-Si + Si-Si, (13)

shows that the bond energy balance boils down to the energy for formation of a $X \cdots H$ steric interaction against that for breaking a X^- -Si bond, plus formation of a remote Si-Si bond against breaking of a H^+ -Si unit in isolated bond centered H^+ . A few assumptions allow us to estimate the dominant chemical contribution to E_b as a function of X. Firstly, Si-Si and H^+ -Si bond energies do not depend on X and can be disregarded. Secondly, and following the ELF analysis, which shows that H is covalently connected to Si, the steric interaction between H and the group-III anion must be relatively weak and should not differ much among different dopants – the calculated distance between X and H varies from 1.3 A for boron to 1.9 A for indium.

The above suggests that a sizable contribution to the variation of E_b with different X should come from changes in the energy of the X^- -Si bond that has to be broken in the reactants side. According to thermochemical data [101], B-Si and Al-Si bonds store respectively 317 kJ/mol and 247 kJ/mol. The contribution of these bonds to the drop in the total energy upon formation of XH is 70 kJ/mol (~ 0.7 eV/pair) larger for X = Al than B. Hence, the cost of breaking the relatively stronger B-Si bond could explain the weaker binding energy of BH in comparison to other XH pairs.

Regarding the second issue – the off-trend dissociation energy of GaH with respect to neighboring AlH and InH – we may find an explanation if we look at the electronic structure of group-III atoms. Unlike the other acceptors, Ga is well known to show a "d-block contraction" effect. This results from incomplete screening of the Ga nuclear charge by its relatively diffuse d-electrons, which enhance the contraction of the outer s and p shells. The radii at which the magnitude of the Al(3s) and Ga(4s) wavefunctions is greatest, are respectively $r_{\rm max} = 1.11$ Å and 1.05 Å [102], clearly reflect this effect. Likewise, wave functions of Al(3p) and Ga(4p) states reach their maximum at $r_{\rm max} = 1.42$ Å and 1.40 Å, respectively [102].

The above facts suggests that Ga-related bonds are slightly shorter than Al-related ones, thus explaining the relatively flatter angle obtained for the Ga-H-Si geometry. The d-block contraction of Ga also explains the formation of shorter and probably stronger Ga-Si bonds for substitutional Ga (calculated as 2.39 Å) in comparison to Al-Si bonds in substitutional Al (calculated as 2.41 Å long), thus justifying the small decrease of the binding energy of GaH with respect to that of AlH.

3. Electronic activity of correlated acceptor-H pairs

The electronic activity of XH pairs was investigated according to Eq. 2. Considering the Si- $H \cdots X$ ground state structures, we did not find transition levels within the gap for any

of the pairs. There must be however a separation between X and H, beyond which passivation is lost and a compensation effect takes over. At this point, the donor level of bond centered H and the acceptor level of X emerge from the crystalline density of states into the band gap. We estimated this effect for the case of B^- - H^+ , by calculating the (-/0) transition of second and third neighboring pairs. During this transition B^- is kept in the negative charge state, while hydrogen changes from H^0 to H^+ . The results show that despite possessing a four-fold coordinated boron atom and a Si-H-Si unit, a second neighboring B^- - H^+ complex is still electrically inactive.

Conversely, third neighboring pairs have a very shallow electron trap, which in the case of B-H is only about 20 meV below the conduction band. This is a (-/0) transition level of the pair, but if we consider the Si-H-Si unit only, this level could be described as a (0/+) transition of H (next to a B⁻ ionized acceptor). For isolated H (infinitely separated from B), the donor transition is calculated at $E_{\rm c}-0.17$ eV, matching the experimentally measured value [103].

The above results, in particular the change of the electronic structure of the pair with respect to that of the isolated components, show that the association of H and X cannot lead to a compensation effect. Combined with the ELF analysis, they indicate that a passivation mechanism takes place via chemical saturation of the Si-H \cdots X structure. Compensation certainly takes place, but only between remote H⁺ and X⁻ species, driving their approach via Coulomb attraction.

4. Dissociation enhancement upon electron capture

The solid black line of Fig. 2(b) replicates the potential energy surface of Fig. 2(a). However, besides describing the energy of H^+ and X^- species, the red line represents the energy of the system upon electron trapping by hydrogen, $X^- + H^+ + e^- \rightarrow X^- + H^0$. With this, we intend to analyze the effect of the presence of a free electron in the conduction band, possibly injected or photogenerated.

Following our discussion above, electron trapping is only possible when H is located beyond the third neighboring bond center site with respect to boron. Electron capture leads to a drop in the energy between 20 meV for close pairs and 0.17 eV for uncorrelated pairs. Hence, some heat is necessary to promote BH separation before any interaction with minority electrons takes place.

Theoretical studies indicate that the diffusivity of neutral hydrogen in silicon is drastically higher than that of H⁺ [13, 17, 91]. The enhancement stems from the minute barrier for motion of metastable H_{AB}^0 along the hexagonal channels of the Si lattice [13, 17]. Recent calculations show that once H⁰ reaches the metastable anti-bonding configuration (overcoming a barrier of $E_m^* = 0.36$ eV), the H atom could travel long distances across a potential landscape that is flatter than the zero-phonon energy of the defect [91]. We note that Fig. 2(b) only shows the higher ($E_m^* = 0.36$ eV) migration barrier, where a jump between two consecutive minima can represent a large traveling distance across the crystalline hexagonal channels.

Recently, B-H and Ga-H pairs were investigated by Fourier-transform infra-red spectroscopy in the context of LeTID [40]. The idea was to monitor the concentration of BH and GaH pairs upon illumination. It was found that the concentrations of the pairs was reduced to 80% of its starting value after low intensity (5 mW/cm²) illumination at room temperature for 96 h.

This picture is consistent with earlier experiments, where the presence of minority carriers was shown to enhance the dissociation of BH pairs in Si [104, 105]. As suggested by Seager and Anderson [104], when free electrons are available, initially the dissociation proceeds with hydrogen as H⁺. However, its subsequent neutralization upon electron capture leads to a marked acceleration of the dissociation process.

This interpretation has been challenged by Herring et al. [16], who did not find any appreciable light-induced dissociation rate of BH, at least up to the temperature of T = 320 K(in Refs. [104, 105] the injection-enhanced dissociation was observed at $T \ge 120$ °C). The authors of Ref. [16] argued that the electron capture by H⁺ next to boron followed by pair dissociation was unlikely. This is because at room temperature and above, the ionization rate of H⁰ is orders of magnitude faster than electron capture, leaving little chance for the shortlived H⁰ atom to escape from B. Fig. 2(b) indeed suggests that the early dissociation steps do not depend on the presence of minority carriers. Some heat is always necessary to break the BH pair. In agreement with Ref. [16], we may conclude that free electrons do not have an impact on the rate of the early reaction $BH \rightarrow B^-$ -H⁺. However, upon annealing and for sufficiently large B-H separations, if we consider an exceptionally fast migration of H⁰ along the hexagonal channels of the Si lattice, the capture of minority electrons by H⁺ could decrease the concentration of BH by smearing the H atoms across the lattice and slowing the recovery of the pairs.

5. Finite-temperature and zero-point motion effects

Density functional theory aims at finding the many-body electronic ground state energy and respective electron density subject to a static external potential at $T=0~\rm K$. It is therefore reasonable to question about the importance of finite temperature effects to the results, for instance, to the calculated reaction energies. Another issue which is worth discussing is the contribution of zero-point motion to the calculated quantities, and by the way, what would be the impact of substitution of hydrogen by deuterium – after all, for practical reasons, H properties are often determined by performing measurements involving the heavier isotope. For instance, the detectivity of D via secondary ion mass spectrometry is nearly two orders of magnitude better than that of H [106]. It is therefore important to understand how reaction energies and barriers depend on the hydrogen mass.

Regarding quantum mechanical effects like tunneling motion of nuclei, in particular of H, they only stand out (in comparison to thermally activated processes) at temperatures that are too low to grant them relevance at room temperature and above. We leave these effects out of the scope of this work.

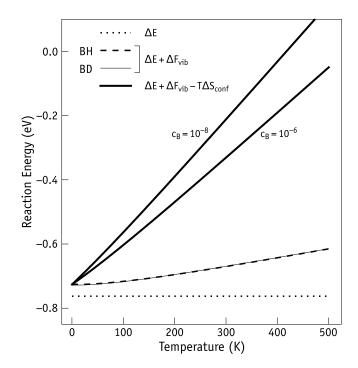


Figure 3. Change in the Helmholtz free energy along the reaction $B^- + H^+ \to BH$ considering the cumulative contributions from the all-electron-ion potential energy (dotted), vibrational free energy (dashed) and configurational entropy (thick solid). The vibrational free energy includes the zero-point contribution. A plot of $\Delta E + \Delta F_{\rm vib}$ for the case of boron-deuterium pair formation (BD) is shown as a solid thin line (almost undistinguishable from the dashed line of BH counterpart). The total free energy change for two typical concentrations of boron in Si are shown (thick solid lines).

Fig. 3 depicts static, dynamic and configurational contributions to the Helmholtz free energy change across the reaction $B^- + H^+ \rightarrow BH$. The contributions are changes in (1) the all-electron-ion potential energy (ΔE) taken from many-body ground state energy calculations within hybrid density functional theory; (2) the vibrational free energy ($\Delta F_{\rm vib}$), including zero-point motion ($\Delta E_{\rm ZP}$), obtained within the harmonic approximation; and also (3) the change in configurational entropy across the reaction ($\Delta S_{\rm conf}$). The calculated free energy of a defect-free supercell had to be considered in the products side of the reaction to comply with stoichiometric balance.

We start by discussing the magnitude of the potential (static) terms. The electron-ion energy change, $\Delta E = -0.76$ eV, is represented by the horizontal dotted line and accounts for most of the reaction energy. Zero-point energy due to atomic vibrations at T=0 K are responsible for $\Delta E_{\rm ZP}=37$ meV only, slightly decreasing the binding energy to $E_{\rm b}=0.72$ eV. The total potential energy change ($\Delta E + \Delta E_{\rm ZP}$) corresponds in Fig. 3 to the value of the dependence shown by the dashed line at T=0 K.

We now look at the effects of temperature and entropy across the $B^- + H^+ \to BH$ reaction. The vibrational free energy, which describes the raise of internal energy with T due to vibrational excitations, the corresponding increase in vibra-

tional entropy, as well as zero point motion, is shown in Fig. 3 as a dashed line ($\Delta E + \Delta F_{\rm vib}$). The changes in vibrational free energy are responsible for the temperature dependence of the reaction free energy ($\Delta F_{\rm vib} \sim 0.12$ eV upon increasing the temperature from 0 K to 500 K).

As for the configurational entropy change per BH defect across $B^- + H^+ \rightarrow BH$, we have (see Appendix A),

$$\Delta S_{\text{conf}} = k_{\text{B}} \ln(2c_{\text{B}}), \tag{14}$$

where $c_{\rm B} = n_{\rm B}/n_{\rm Si}$ is the fractional concentration of boron, $n_{\rm B}$ and $n_{\rm Si}$ being respectively the number of B dopants and Si sites in a crystalline sample. As expected, the configurational entropy change across the reaction is negative, thus favoring the reactants side with raising the temperature. We are now in a position to estimate the temperature above which BH is not stable anymore, and that is when $\Delta F = \Delta E +$ $\Delta F_{\rm vib} - T \Delta S_{\rm conf} = 0$. Taking a reference doping concentration in the range $c_{\rm B}=10^{-8}\text{-}10^{-6}$ (corresponding to [B] = $5\times10^{14}\text{-}5\times10^{16}$ cm⁻³ and resistivity $\rho=27\text{-}0.35~\Omega\text{cm}$), we have $\Delta S_{\rm conf} = -(1.52\text{-}1.13)$ meV/K. The contribution of $-T\Delta S_{\text{conf}}$ to the free energy change corresponds in Fig. 3 to the difference between ΔF (solid lines) and $\Delta E + \Delta F_{\text{vib}}$ (dashed line). It can be seen from the figure that the reaction becomes isothermic ($\Delta F = 0$) at approximately $T \approx 450$ K (or about 180 °C). This temperature is just in the middle of the range, 140-220 °C, where the dissociation of BH pairs and recovery of electrical activity of boron atoms occurred in float-zone-grown Si:B crystals at equilibrium conditions (in the dark) [105].

We also investigated the effect on the reaction energy of $B^- + H^+ \to BH$ upon replacing hydrogen by deuterium. The electronic potential energy and the configurational entropy of a defect population are not sensitive to isotope change. Only zero-point motion effects and the vibrational free energy depend on the mass of the nuclei. The change of the free energy across $B^- + D^+ \to BD$ is shown in Fig. 3 as a thin solid line, which is better distinguishable from that related to BH formation (dashed line) close to $T \sim 0$ K, essentially reflecting small differences in zero-point energy. The zero-point energy change for the deuterium reaction is $\Delta E_{ZP} = 0.34$ meV, only 3 meV smaller than the same quantity for the hydrogen analogous reaction. Unaccounted anharmonic effects, which are larger in H-related defects, could slightly increase the difference.

We find two reasons that explain an almost identical temperature dependence of H- and D-related reaction energies: (1) the high energy of hydrogen-related vibrational frequencies; (2) the extreme localization of hydrogen-related vibrational modes. Typical Si-H and Si-D vibrational frequencies in the range 1500-2000 cm⁻¹ correspond to energy quanta of about 7-10 times k_BT at room temperature. The first excited state of these vibrations becomes populated above several hundreds of Kelvin, and any meaningful *mass-related difference* in the contribution to vibrational entropy (or to the vibrational free energy) is felt above thousands Kelvin only. On the other hand, excited states of low energy modes are easily accessible and can play a significant role in the reaction

entropy change. These include strain-induced modes which overlap many crystalline atoms. However, the virtually identical strain field around H and D defects, combined with the extreme localization of the H (and D) modes implies that these *diffuse* vibrations are effectively similar and decoupled from the H (and D) atom.

C. Interactions of H₂ molecules with acceptors, carbon and oxygen

We now turn to the interactions of interstitial hydrogen molecules with p-type dopants and two impurities commonly abundant in silicon materials, namely substitutional carbon (C) and interstitial oxygen (O). We start by discussing medium range interactions between correlated X and H_2 pairs separated by up to ~ 20 Å. Then we will look at short-range interactions, including molecular dissociation next to the impurities.

1. Strain interactions

Hydrogen molecules are electrically inactive and are not subject to long-range Coulomb attraction/repulsion by charged impurities. In floating zone material, where the concentration of oxygen and carbon are usually about 10¹⁶ cm⁻³ or even less, H2 molecules represent most of the hydrogen stock available in samples exposed to a hydrogen source at high-temperatures and subsequently quenched [37, 38]. Isolated molecules are located at tetrahedral interstitial sites of the Si lattice, and they become mobile at temperatures slightly exceeding 300 K [39]. In Cz-Si, most of the molecules are trapped near abundant oxygen impurities, forming close O-H₂ pairs [37]. Here, annealing between room temperature and 160 °C leads to reversible displacement of the equilibrium between the reactants and products sides of O-H₂ \rightleftharpoons O + H₂ [39]. As the molecules migrate across the silicon, they are subject to the strain fields of several impurities and dopants dissolved in the lattice, and that is what we detail in the following paragraphs.

Interactions between H_2 and impurities/dopants were investigated by placing H_2 on all symmetry-irreducible tetrahedral sites of a 512-atom supercell with respect to a specific impurity/dopant. Nearly 30 sites in total were identified.

Fig. 4 shows the relative energy of H_2 -impurity/acceptor pairs as a function of their separation, r (upper horizontal axis). The zero energy in the vertical axis is set to the state where the molecule is infinitely separated from the dopant/impurity. The elastic potential between defects decays as r^{-3} [107] and that is how we define the scaling of the lower horizontal axis. The scatter in the plots can be essentially attributed to the atomistic-range interactions within the cubic host (not described by elasticity), and to the anisotropy of interstitial oxygen. Based on its minute barrier for rotation (few meV), effects from the elastic anisotropy of the H_2 molecule are deemed very small.

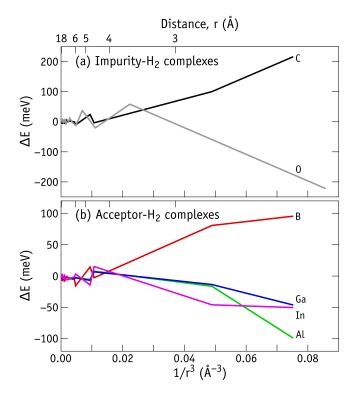


Figure 4. Energy of (a) impurity- H_2 pairs and (b) acceptor- H_2 pairs in silicon as a function of the distance between the impurity/acceptor and the molecule. Impurities considered are substitutional carbon (C) and interstitial oxygen (O), both being electrically inactive. The acceptors (B, Al, Ga, In) were all in the negative charge state. The zero energy corresponds to the state of uncorrelated pairs.

Fig. 4(a) depicts the results for H₂ interactions with C and O. The first conclusion is that these two defects interact rather differently with the molecules. While C is repulsive, O is attractive. This could explain the observations in Cz-Si, where after high-T hydrogenation treatments with subsequent quenching, H₂ is trapped next to oxygen impurities. Our interpretation of these results agrees with early calculations of Hourahine et al. [108], where it was found that bond centered O expands the volume of the six equivalent nearest tetrahedral interstitial sites, making them preferential for the molecule. Conversely, the short C-Si bonds create a tensile elastic field around carbon, tightening the volume of close interstitial sites, thus raising the energy of the resulting complexes.

Another interesting conclusion is that the interaction energy decreases very quickly, converging toward below $k_{\rm B}T$ at room temperature for distances of $r\gtrsim 5$ Å only. This is the magnitude of a typical capture radius for defect reactions in the absence of electrostatic interactions.

The calculated binding energy $E_{\rm b}=0.22~{\rm eV}$ for O-H₂ is in good agreement with the experiments of Markevich and Suesawa [39], who derived 0.28 eV for this quantity. Accordingly, H₂ molecules were formed after quenching O-rich Si that was previously put in contact with hydrogen gas at 1200 °C. The molecules were found to be mobile at about room temperature and became trapped next to O impurities. At slightly higher temperatures, $T \gtrsim 50~{\rm eC}$, the O-H₂ complexes disso-

ciated, making the molecules available to participate in other reactions [39].

Weak interactions were also found for acceptor- H_2 pairs. Again, the tensile species (B) is repulsive for the molecules, whereas compressive elements (Al, Ga, In) have larger X-Si bonds and increase the open volume of their six equivalent first neighboring interstitial sites. The binding energy is rather week (< 0.1 eV) and the trend obtained may also reflect the electronic radius of each individual species. Interestingly, the strongest repulsive effect of carbon could suggest a preferential interaction between H_2 and boron, even when comparable quantities of both impurities are present [38].

2. Dissociation of H_2 molecules next to dopants and carbon

We recently estimated that, in the absence of a catalyst for H_2 dissociation, the molecules should survive up to about 400 °C in pristine Si [91], well above the annealing temperature of H_2^* dimers (~ 200 °C) [109]. The dissociation of the molecule in a crystalline region of the Si was suggested to occur upon collision of H_2 with a Si-Si bond, possibly leading to the transient formation of metastable H_2^* before dissociation. The activation potential energy for the process was evaluated (using the same methodology employed in this work) as $E_a = 1.62$ eV.

We investigated a similar reaction, but next to a boron impurity. Likewise, the reaction between H_2 and substitutional carbon was investigated for the sake of comparison. Carbon is well known to interact with hydrogen and form stable CH_2 defects. Therefore, it can compete with boron for the capture of H_2 . The CH_2 complexes are electrically inert and stable up to $T \sim 250$ °C [110]. According to previous theoretical work [17, 111, 112], the most stable form of the defect is illustrated in Fig. 5(c). The structure comprises a pair of \equiv C-H and \equiv Si-H units aligned along a common trigonal axis, where the H atom connected to carbon lies close to the center of a broken C-Si bond, while the H atom connected to Si is at the anti-bonding site to the same broken C-Si bond.

We looked at two reaction sites for H_2 next to boron. They involved the overlap of the molecule either with first or second neighboring bonds to the B atom (B-Si or Si-Si bonds, respectively). The mechanism is almost identical in both cases, and they can fork into reactions such as (1) $H_2 + B^- \to BH_2^-$; (2) $H_2 + B^- + 2h^+ \to BH_2^+$; or (3) $H_2 + 2B^- + 2h^+ \to 2BH$. In (1) and (2) we are implicitly anticipating that we found stable negatively and positively charged BH_2 states. So far, the acceptor state has been unreported. The donor state, on the other hand, was recently identified by de Guzman *et al.* [59].

We found that the barrier along the minimum energy paths for the above reactions involves the dissociation of H_2 next to first neighboring B-Si bonds. Figs. 5(a) and 5(b) help us to visualize the early stages of the dissociation mechanism. They depict the structures respectively before and after the transition state. The initial state, comprising a molecule at the tetrahedral interstitial site next to boron is shown in Fig. 5(a). The molecule then moves toward the B-Si bond, attaining the

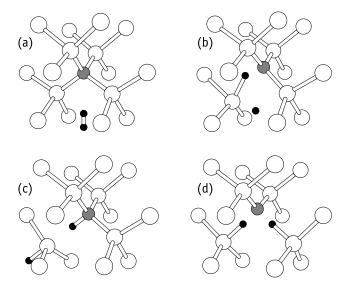


Figure 5. Mechanism for the dissociation of a H_2 molecule next to a boron impurity and stable BH_2 complexes in silicon. (a) Initial configuration with H_2 at the tetrahedral interstitial site next to boron. (b) Metastable configuration after overcoming the saddle point for dissociation. (c) Stable acceptor state of BH_2 . The most stable CH_2 complex is analogous, with boron being replaced by carbon. (d) Stable donor state of BH_2 . Si, B and H are shown in white, gray, and black, respectively.

state shown in Fig. 5(b). The latter is a local minimum of energy at 0.49 eV above the initial state. The transition state between the two configurations is 1 eV above the initial state. To find the actual dissociation barrier of H_2 upon reaction with B^- , we have to consider the 0.1 eV offset between a close B^- H₂ pair and infinitely separated $B^- + H_2$ (*c.f.* Fig. 4(b)). The activation energy for H_2 dissociation next to B is therefore $E_d = 1.1$ eV, nearly 0.5 eV lower than the analogous quantity in pristine silicon (without the assistance of the dopant). Note that the calculated dissociation barrier is larger than the energy barrier that H_2 needs to surmount in order to migrate and get close to the B^- ion (0.78 eV [39]).

The metastable state of Fig. 5(b) comprises a complex made of a neutral BH pair next to a ${\rm H^-}$ anion located close to the tetrahedral interstitial site. Let us refer to it as $({\rm BH\text{-}H^-})^*$. From here, several fast processes can take place, including ${\rm H^-}$ relocation through a close hexagonal ring to form ${\rm BH}_2^-$ as depicted in Fig. 5(c). The calculated barrier for this step is 0.50 eV high, and overcoming it leads to completion of reaction (1) referred above. Other possibilities may follow from the capture of holes by stable ${\rm BH}_2^-$ or metastable $({\rm BH\text{-}H^-})^*$ states. This could lead either to formation of ${\rm BH}_2^+$ (reaction 2), whose ground state geometry is depicted in Fig. 5(d), or to the escape of neutral hydrogen from $({\rm BH\text{-}H^0})^*$, which can subsequently capture a further hole and react with another ${\rm B}^-$ impurity (reaction 3).

The kinetics of formation and dissociation of BH pairs was recently investigated during dark annealing treatments of floating-zone B-doped Si wafers, passivated with silicon nitride on both faces, and subject to a firing treatment [44]. Ac-

tivation energies for formation and dissociation of the pairs of 1.29 eV and 1.22 eV were extracted from the data cast in Arrhenius plots [44]. These figures are close to our calculated dissociation barrier of H_2 next to B^- , and dissociation energy of a BH pair, 1.1 eV and 1.2 eV, respectively. We note that the theoretical barrier is a high bound of the true barrier. An alternative mechanism with lower transition state energy could have escaped our search. That would explain the lower activation energy (0.84 eV) for the formation rate of BH pairs (from reaction between H_2 and boron) that was measured by Walter et. al. [45].

In another recent experiment, Acker et al. [49] studied the H₂ dissociation dynamics, and subsequent formation of BH and GaH pairs in floating-zone Si doped with boron and gallium, respectively. Activation energies of $E_a = 1.20 \pm 0.02$ eV and $E_a = 1.04 \pm 0.01$ eV were found for the formation rate of BH and GaH pairs, respectively. The first figure is again very close to the calculated B-assisted dissociation barrier of the molecule ($E_d = 1.1 \text{ eV}$). We did not calculate the Gaassisted dissociation barrier of H₂. However, considering that (i) unlike boron, gallium does not show a repulsive strain field for the reaction with H₂ (the repulsive barrier is 0.1 eV for boron c.f. Fig. 4), and that (ii) judging from the similar pre-exponential factors measured for BH and GaH formation $(\sim 4 \times 10^{-8} \,\mathrm{s}^{-1})$ [49], both pairs are likely to share the same formation mechanism, the calculated barrier for dissociation of H₂ when the molecule is already next to boron (1 eV), could represent a good approximation for the analogous figure involving the formation of GaH pairs.

Regarding the reaction between H₂ and substitutional carbon, the barrier for molecular dissociation next to the C-Si bond was estimated as $E_{\rm d}=1.15$ eV. The mechanism for the $C + H_2 \rightarrow CH_2$ reaction is analogous to that involving boron. However, the metastable state attained after overcoming the dissociation barrier, consists of a rather stable structure $(C-H\cdots H-Si)^*$, with energy -0.7 eV below the initial state. Here, a C-Si bond is converted into C-H and H-Si bonds, resulting in an electrically inert structure which cannot interact with holes. The geometry of $(C-H \cdots H-Si)^*$ is non-linear with C and Si bond angles showing substantial deviations from the tetrahedral sp³ geometry. Again, adding to the above barrier the 0.2 eV off-set between the energies of the neighboring C- H_2 pair and uncorrelated $C + H_2$ (c.f. Fig. 4(a)), for the reaction $C + H_2 \rightarrow CH_2$ we end up with a carbon-assisted H_2 dissociation barrier of $E_{\rm d} = 1.35$ eV.

CH₂ complexes have been observed and studied in the past [17, 111–114]. They quickly form during the fast cooling that is applied after soaking C-rich silicon in H₂ gas at around 1200 °C. However, we do not really know if the complexes form upon sequential capture of H ions by carbon, or if they result from direct reaction between C and H₂ molecules. Certainly, an interesting observation is that if we start from asquenched H₂-soaked boron-doped Fz-Si, subsequent annealing treatments lead to (partial) loss of H₂ molecules, and a concomitant raise in the concentration of BH pairs (see Fig. 2 of Ref. [38]). However, in carbon rich Fz-Si there seems to be no reactions between H₂ molecules and C upon similar treatments (see Fig. 3 of Ref. [113]). In the latter case the CH₂

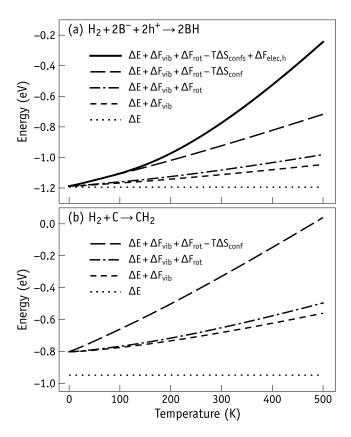


Figure 6. Cumulative contributions from the electron-ion potential energy (dotted), vibrational free energy (dashed), rotational free energy (dashed-dotted), configurational entropy (long dashed) and hole free energy (solid) to the change in the Helmholtz free energy (ΔF) along the reactions (a) $\rm H_2 + 2B^- + 2h^+ \rightarrow 2BH$ and (b) $\rm H_2 + C \rightarrow CH_2$. The vibrational free energy accounts zero-point motion effects. Fractional concentrations $c_B = c_C = 10^{-6}$ and $c_H = 10^{-8}$ were considered for the evaluation of configurational and electronic entropy (see Appendix D).

complexes are already formed in as-quenched samples, and annealing leads to a decrease in their concentration only. Further details on interactions between H_2 and C will be dealt with in a separate paper.

It is useful to compare the most favorable reactions in p-type Si involving H_2 with either boron or carbon. The reaction $H_2 + 2B^- + 2h^+ \rightarrow 2BH$ is the one that maximizes the potential energy drop, corresponding to $\Delta E_R = -1.19$ eV. Conversely, in carbon-rich material H_2 is known to interact effectively with substitutional carbon, and in that case, the reaction is $H_2 + C \rightarrow CH_2$ with $\Delta E_R = -0.94$ eV, where CH_2 stands for a neutral complex with a geometry identical to that shown in Fig. 5(c). Hence, from the perspective of the potential energy drop (at T=0 K), both forms of hydrogen defects, namely BH pairs and CH_2 complexes, show comparable stability, perhaps with a slight advantage to the BH pairs.

Fig. 6 shows the cumulative contributions of several degrees of freedom to the free energy change along reactions (a) $H_2 + 2B^- + 2h^+ \rightarrow 2BH$ and (b) $H_2 + C \rightarrow CH_2$. In both

cases, hydrogen is in the molecular form on the reactants side. This implies that the energy reference of the products is the same. The scaling of the axes was also made identical in both plots. At first glance, we obviously note that the zero-point energy change for reaction (a) is insignificant when compared to about 0.15 eV in reaction (b). This is shown by the energy offset that separates the electron-ion potential change ΔE (obtained within hybrid density functional theory and represented as a dotted line) from the other terms at T=0 K. This effect makes (b) less favorable, and to great extent, is due to formation of stiffer and higher frequency C-H and Si-H oscillators with wag modes in CH₂, against the two softer Si-H oscillators with very low-energy wag modes in 2BH. Another important aspect that favors BH formation in detriment of CH₂ is the larger drop in configurational entropy in (b) than in (a) (compare long dashed lines in Figs. 6(a) and (b)), so that $-T\Delta S_{\text{conf}}$ for BH pair formation grows slower with increasing the temperature.

Reaction (a) involves the passivation of two shallow acceptors, and above the carrier freezeout temperature of Bdoped Si (~ 80 K), it also involves the subtraction of two free holes per H₂ molecule. We estimated the electronic free energy per hole ($\Delta F_{\rm elec,h}$) added to the electronic thermal bath of the sample. A change in the free hole density $\Delta p = c_{\rm H}[{\rm Si}] = 5 \times 10^{14} {\rm cm}^{-3}$ was considered, where [Si] is the density of Si atoms in crystalline Si in units of cm⁻³, and that corresponds to a full conversion of the available molecules ($c_{\rm H}=10^{-8}$) into BH pairs (the total boron available was $c_{\rm B} = 10^{-6}$). Details of the calculation are presented in Appendix D. The total free energy change (accounting for electronic, vibrational, rotational, and configurational freedom) is represented in Figs. 6(a) as a solid thick line. It is clear that despite the rapid increase in the free energy change with increasing the temperature, the free energy drop for $H_2 + 2B^- + 2h^+ \rightarrow 2BH$ is invariably larger than that for CH₂ formation shown in Fig. 6(b).

We suggest that during the cooling of the Si, either after being subject to a high temperature treatment in contact with hydrogen gas, or upon firing a passivated Si structure covered by a H-rich passivating layer (like in the fabrication of solar cells), H_2 molecules formed within the bulk are more likely to react with boron than carbon, unless the concentration of the latter is dominant.

The above conclusion is supported by both the smaller barrier for the reaction of H_2 with B and the larger free energy drop per molecule upon BH pair formation. It is also in line with the observed H_2 reactions in different types of S in materials quenched from high temperature treatments in H_2 gas. In cast multicrystalline material, where carbon concentration is typically in the range $[C] \sim 10^{17} \cdot 10^{18}$ cm⁻³, most hydrogen in as-quenched samples is found connected to carbon in the form of CH_2 defects [114]. On the other hand, in boron doped floating zone Si with $[C] \lesssim [B] = 10^{16}$ cm⁻³, as-cooled samples contained mostly isolated H_2 with 5% of the hydrogen already in the form of BH pairs [38]. Annealing at 160 °C was sufficient for the molecules to travel and overcome the reaction barrier (calculated here as 1.1 eV) before intimate reaction with boron took place. A 1:1 correlation between the loss of

molecular hydrogen and formation of BH was found. Finally, in C-lean n-type Cz-Si, the molecules are found trapped next to abundant O_i impurities (where the binding energy of H_2 to oxygen was measured as 0.26-0.28 eV) [37, 39]. One puzzling observation in the B-doped floating zone samples was that only about 50% of molecular hydrogen was "consumed" during the conversion into BH pairs. A saturation of the reaction was attained after about 24 hours at 160 °C [38].

3. Electronic structure of acceptor-H₂ complexes

As briefly disclosed already, BH₂ can be both a donor and an acceptor. The BH₂⁺ donor state consists of two H atoms sitting at the center of neighboring B-Si bonds. The atomistic geometry of the donor, hereafter denoted as D is depicted in Fig. 5(d) and comprises two Si-H bonds next to undercoordinated boron. The one-electron structure of the neutral state for this configuration shows a high-lying highest occupied Kohn-Sham state edging the conduction band bottom.

Regarding the acceptor state, we found two stable BH_2^- geometries which resemble the H_2^* complex. However, here the boron atom replaces one of the two inequivalent Si atoms connected to H, leading either to $B\text{-}H_{BC}\cdots Si\text{-}H_{AB}$ or $Si\text{-}H_{BC}\cdots B\text{-}H_{AB}$ configurations. They are respectively referred to as A and A'. The first is depicted in Fig. 5(c) and it is more stable than A' by 0.13 eV. In their neutral charge states, both geometries lead to the appearance of a lowest unoccupied Kohn-Sham state edging the valence band top, strongly indicating that they are shallow acceptors.

In line with a recent report by us [59], the donor transition involving electron emission from neutral BH $_2^0(D)$ to the conduction band, $D^0 \rightarrow D^+ + e^-$, is calculated at $E_c - 0.19$ eV. In that study we were unaware of other configurations. We now found that A^0 is 0.43 eV more stable than D^0 , so that the actual donor transition should be close to mid-gap, at $E(A^0/D^+) - E_v = 0.48$ eV and involves two different structures

As for the acceptor states (involving either structure A or A'), we found them to be very shallow. A direct comparison of their electron affinities with the same quantity for boron, leads us to the conclusion that A and A' defects are shallow acceptors with (-/0) transitions very close to $E_v + 40$ meV. We can understand this result by noting that boron in A and A' complexes is four-fold coordinated.

Combining the shallow acceptor levels with the estimated location of the donor transition, we find that BH_2 is a negative-U complex with a metastable neutral state. The (-/+) transition of BH_2 is calculated at $E(A^-/D^+)-E_v=0.26$ eV, so that when the Fermi energy is below (or above) this level, the complex is most likely to be found in the $BH_2^+(D)$ (or $BH_2^-(A)$) state [72].

Dihydrogenated complexes with larger acceptors (XH_2 with X = AI, Ga, In) also show amphoteric and negative-U character. For the donor state, the Si-H bonds notably deviate away from $\langle 111 \rangle$ directions, implying that the bond angles be-

Table II. Electronic transition levels and reaction energies of XH_2 complexes in Si. The electronic transitions are indicated graphically in Figure 7. The energy of metastable $BH_2^-(A')$ configuration with respect to that of $BH_2^-(A)$ is also shown.

Acceptor (X)	В	Al	Ga	In
${E_{\rm c}-E({\rm D}^0/{\rm D}^+)}$	0.19	~ 0	~ 0	~ 0
$E(A^0/D^+) - E_{\rm v}$	0.48	1.20	1.15	1.29
$E(A'^0/D^+) - E_v$	0.61	1.38	1.49	1.80
$E(A^-/A^0) - E_{\rm v}$	0.04	0.06	0.06	0.12
$E(A'^-/A'^0)-E_{\rm v}$	0.04	0.08	0.07	0.17
$E(A^-/D^+)-E_v$	0.26	0.63	0.61	0.71
$XH_2^-(A) \rightarrow XH_2^-(A')$	0.13	0.20	0.35	0.55
$2XH \rightarrow X_s^- + XH_2^+(D)$	0.36	0.39	0.43	0.38
$XH + H^+ \rightarrow XH_2^+(D)$	-0.40	-0.57	-0.48	-0.57
$\mathrm{H}_2 + X_\mathrm{s}^- \to X \mathrm{H}_2^-(\mathrm{A})$	-0.31	0.07	0.14	0.22
$X_{\rm s}^- + {\rm H}_2 + 2{\rm h}^+ \to X{\rm H}_2^+({\rm D})$	-0.83	-1.19	-1.07	-1.19
$\frac{2X_s^- + H_2 + 2h^+ \rightarrow 2XH}{}$	-1.19	-1.58	-1.50	-1.58

tween the Si atoms (connected to H) and their ligands, display some variations with respect to the perfect tetrahedral geometry. As for the $XH_2^-(A')$ defects, they are also metastable with respect to $XH_2^-(A)$, respectively by 0.20, 0.35 and 0.55 eV for X=Al, Ga, and In. Notably, two aspects distinguish the heavier XH_2 complexes from BH_2 . First, D^0 defects were found to ionize *spontaneously*, with the electron on the highest occupied state being spread over a conduction-band-like state. This is a strong indication of an effective-mass-like donor defect. Second, the negative-U transition levels for the heavier XH_2 complexes were found in the upper part of the gap, namely, $E(A^-/D^+) - E_v = 0.6$ eV for AlH2 and GaH2, whereas $E(A^-/D^+) - E_v = 0.7$ eV for InH2. The calculated electronic transitions for all XH_2 complexes are summarized in Tab. II.

4. Transformations and reconfigurations involving BH₂ complexes

Considering the charge-dependent geometry of BH₂, it is instructive to have a close look at possible transformations of this complex, eventually involving the capture or emission of carriers. Fig. 7 represents a configuration coordinate diagram of possible reactions and transitions involving B and H in p-type silicon. The far right and left of the CCD represent molecular hydrogen (away from boron) and dissociated hydrogen molecules (paired with boron), respectively. Between these two states, several reactions were considered, including the formation of BH₂ complexes in the middle region. Energies of local minima are represented below each potential basin along with the respective chemical formula. Some of these figures were already discussed above. The zero energy of the left (lower) part of the CCD is the 2BH state. Conversely, the zero energy of the right (upper) part of the diagram is the $2B^- + H_2 + 2h^+$ state. These are separated by 1.19 eV, representing the energy gain per molecule after full

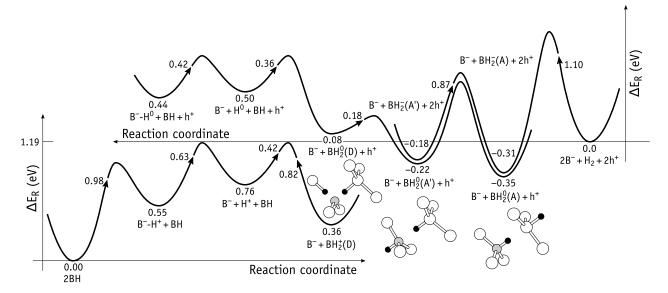


Figure 7. Configuration coordinate diagram of two substitutional boron and two hydrogen atoms in silicon. Upper and lower diagrams have zero energies for $2B^- + H_2 + 2h^+$ and 2BH states, respectively, which are separated by 1.19 eV. Energies (in eV) of stable states are shown at the bottom of each local minimum. Transition/reaction barriers are indicated next to arrow heads, and they are relative to the nearest local minimum. Atomistic structures of BH_2 complexes are presented next to their respective energy minima. Si, B and H atoms are shown in white, gray and black, respectively.

passivation of boron. This result is close to the measured activation energy $E_a = 1.35 \pm 0.15$ eV of the equilibrium constant of the reaction $H_2 + 2B^- + 2h^+ \rightleftharpoons 2BH$ in boron-doped Si [45]. Fig. 7 also shows several transformation barriers that were calculated from transition state energies with respect to the basin of the corresponding initial states. The energy barriers are indicated next to the arrow heads.

Much of the left part of the CCD of Fig. 7 has been described in Sec. III B and detailed in Fig. 2. The dissociation energy of BH was estimated as 1.2 eV. However, under above-band-gap illumination or carrier injection, the breaking of BH into a close B⁻-H⁺ pair involves surmounting a barrier of 0.98 eV, and when H⁺ reaches the third neighboring bond center site from boron and beyond (at least 0.55 eV above the left-reference state), photogenerated or injected electrons can be trapped by H⁺, facilitating the escape of H⁰ from the ionic Coulomb field of B⁻. Also, as pointed out already, during individual jumps, H⁰ atoms attain a metastable state in the open interstitial regions of the lattice, where the potential energy for motion is flatter than the zero-point energy. This implies that this species can travel long distances athermally [91].

The right end of the CCD of Fig. 7 describes the interaction between the molecules and boron. Dissociation of H_2 assisted by B involves surmounting a barrier of 1.1 eV, possibly leading to formation of one BH pair plus release of H^+ , which can subsequently react with B^- . However, as we saw in Sec. III C 2, it can also result in immediate formation of $BH_2^-(A)$, or $BH_2^+(D)$ upon reconfiguration and capture of holes. The potential energy barriers between BH_2 structures are relatively small, especially the one separating $BH_2^0(A')$ from $BH_2^0(D)$. This amounts to 0.18 eV only, resulting from the displacement of one of the H atoms in $BH_2^0(D)$ to the

anti-bonding site with respect to the B atom. The conversion from $BH_2^-(A')$ into $BH_2^-(A)$ starts with the dissociation of the B-H bond in $BH_2^-(A')$, followed by the displacement of the loose H^- anion through hexagonal sites to end up at the anti-bonding site next to the Si-H unit. The first step of this mechanism involves surmounting a barrier estimated as 0.87 eV. The barriers for subsequent jumps of H^- are about 0.5 eV high [91]. Of course, at room temperature and above, once the B-H bond is broken, H^- is also likely capture two holes to become H^+ at the bond center, escape from the neutral BH pair, and finally be captured by B^- .

From our results we conclude that H_2 can dissociate upon interaction with B^- , and that there is a strong thermodynamic drive for dispersion of H in the form of BH pairs. Of course, BH_2^- and BH_2^+ are possible intermediate species along the $2B^- + H_2 + 2h^+ \rightarrow 2BH$ reaction.

Fig. 8 provides a qualitative picture of the thermal stability of several relevant states comprising a population of hydrogen and boron atoms in silicon. Concentrations of substitutional B and interstitial H were assumed to be 10^{-6} and 10^{-8} , respectively. These quantities enter in the evaluation of configurational and electronic entropy of holes. The figure depicts the temperature dependence of the free energy when all H is paired with B (2BH), when it is dissociated from B and dispersed in the form of protons $(2B^- + 2H^+)$, and when it forms boron-dihydrogen complexes $(B^- + BH_2^+)$ and $B^- + BH_2^- + 2h^+)$. All free energies are represented with respect to a common reference state $2B^- + H_2 + 2h^+$ (shown as a horizontal line).

In the analysis of Fig. 8 we should bear in mind several approximations considered. Among these we highlight (i) the

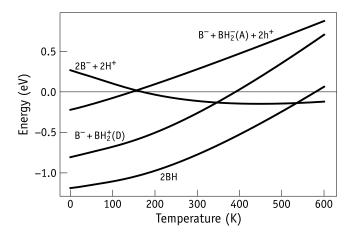


Figure 8. Temperature dependence of the free energy of some relevant states involving a population of hydrogen and boron atoms in silicon, with respect to the free energy of the $2B^- + H_2 + 2h^+$ state (represented by the horizontal line at zero energy). Configurational and electronic entropy contributions were estimated by assuming concentrations of substitutional B and interstitial H of 10^{-6} and 10^{-8} , respectively.

assumption of a low concentration of impurities and the neglect of impurity-impurity interactions; (ii) that H impurities and complexes are all in the same form (for instance, in the 2BH state all hydrogen atoms are paired with boron while unpaired boron atoms occupy substitutional positions); (iii) limitations in the approximated treatment of configurational and electronic entropy.

Fig. 8 shows that at T=0 K the 2BH state is 1.19 eV below the $2B^- + H_2 + 2h^+$ reference. This was already shown in Fig. 7. With increasing temperature BH becomes unstable with respect to dispersed H⁺ at $T \gtrsim 500$ K. The main drive for the stabilization of the $2B^- + 2H^+$ state is the dilution of hydrogen and the corresponding entropy increase. It is noteworthy that the diagram cannot (and does not attempt to) explain the formation of free molecules in hydrogenated Si quenched from high temperatures – the reference state $(2B^- + H_2 + 2h^+)$ is metastable with respect to $2B^- + 2H^+$ above 150 K. On the other hand, H2 formation is a nonequilibrium process. As proposed in Ref. [91], the free energy of formation of interstitial H⁻ is reduced at high temperatures and a small population of the anion is expected to show up. Combined with a larger configurational entropy of the $H^+ + H^-$ mix, a stabilization effect was proposed, allowing for the molecules to form via Coulomb attraction between oppositely charged ions. This effect deserves further investigation of its own.

Regarding the BH_2 complexes, they display a low thermal stability. As shown in Fig. 8, the relative free energy of the acceptor state ($B^- + BH_2^- + 2h^+$) becomes positive well below room-temperature. This applies to p-type Si and it means that the reaction of the molecule with B^- (without involvement of holes) is not favorable. If formed temporarily, BH_2^- complexes are likely to dissociate or capture holes to end up in BH_2^+ . The difference between the T-dependence of the free energies of $B^- + BH_2^- + 2h^+$ and $B^- + BH_2^+$ states, mostly

comes from the contribution of electronic entropy. The donor state has less entropy due to capture of two holes. This state is also metastable against 2BH across the whole temperature range, and if formed, it has a barrier of only 0.82 eV preventing its dissociation into more stable BH complexes (c.f. Fig. 7). Hence, thermal dissociation of BH $_2^+$ and further formation of BH pairs is likely to take place close to room temperature.

The BH $_2^+(D)$ defect was recently suggested to be responsible for an electron trap at $E_{\rm c}-0.175$ eV (referred to as $E_{0.175}$) in n-type Si co-doped with boron [59]. The observation of a pronounced Poole-Frenkel effect suggested that $E_{0.175}$ relates to a donor transition. Our results support that conclusion — we estimate the donor transition of BH $_2(D)$ to be located at 0.19 eV below $E_{\rm c}$. Annealing experiments have shown that $E_{0.175}$ starts to anneal out above 280 K under open-circuit conditions [115]. This observation also agrees with the finite temperature results in Fig. 8, which indicate that BH $_2^+$ should dissociate into B $^-$ + 2H $^+$ at about room temperature.

In n-type Si the lowest state of BH_2 is the shallow acceptor $BH_2^-(A)$ and not the donor state. However, in p-type material the calculated thermal instability of BH_2^- indicates that this state cannot form (being less stable than $B^-+H_2)$ above ~ 100 K. Hence, above this temperature, BH_2 should be effectively viewed as donor defect (without an acceptor) for a wide temperature range.

We finally point to the calculated potential energy changes pertaining to the $2B^- + H_2 + 2h^+ \rightarrow 2BH$ reaction, including intermediate complexes, summarized at the bottom of Tab. II. Analogous quantities are reported for the same reactions involving heavier acceptors (X = Al, Ag, In). Although we did not investigate reaction transition states for $X \neq B$, based on the reaction energetics reported in Table II we find that the CCD of Fig. 7 can be applied to the heavier dopants as well, if we make a few adjustments. Several features/differences are highlighted: (i) The $X^- + XH_2^+$ state is in general metastable by approximately 0.4 eV with respect to the 2XH ground state; (ii) Unlike in B-doped material, formation of the shallow acceptor $XH_2^-(A)$ states (with X = Al, Ga, In) upon reaction between H_2 and X^- is endothermic already at T = 0 K; (iii) Like for the XH pairs, XH_2^+ has a smaller binding energy in B-doped Si, either with respect to the release of molecules $(X^- + H_2 + 2h^+)$, or to the release of protons $(XH + H^+)$; and finally (iv) whereas BH_2^+ is a deep electron trap, other XH_2^+ complexes are effective-mass-like shallow donors. Regarding this latter aspect, Ref. [115] provides a proposal for the non-radiative recombination mechanism involving the BH₂⁺ complex, and a comparison with heavier {Al,Ga,In}H₂⁺ complexes.

D. Local vibrational modes of boron-hydrogen complexes

In this section, we explore the LVM frequencies of boronhydrogen complexes and their connection to the observations. The frequencies are summarized in Tab. III and they are accompanied by their calculated oscillator strengths. These can be related to the relative amplitude of the corresponding infrared absorption peaks. Due to the harmonic approximation, the calculated frequencies tend to be overestimated [116]. To facilitate the comparison between theory and measurements, computed frequencies are often shifted or scaled, typically by a factor $\lambda \gtrsim 0.9$ [117]. This effect is paradigmatic for Si-H stretching oscillations, whose frequencies are often overestimated by more than $100~\text{cm}^{-1}$ (see Tab. 1 of Ref. [118] which reports values of Si-H related modes of vacancy-hydrogen complexes in Si).

On the other hand, the quality of the description of the electron-electron interactions for the calculation of the interatomic dynamical matrix is also important. Here we use the GGA, which is known for underestimating bond strengths, and consequently to soften the frequencies. The overall error with respect to the measurements depends mostly on the relative weight of the two opposite effects. Hence, a practical and often used approach for better locating the frequencies is to calculate the frequency deviation with respect to an experimentally well-characterized defect mode (for instance a Si-H vibration in a VOH complex), and expect a similar deviation for analogous modes in other defects (for instance a Si-H vibration in VH).

The errors in the calculations can also show variations even when dealing with defects that solely differ on the mass of one of its elements (*e.g.* isotope substitution). A bond-centered proton has a calculated frequency for the asymmetric stretching mode of the Si-H⁺-Si unit of 2082 cm⁻¹. Experimentally, this was attributed to a peak at 1998 cm⁻¹ in infra-red absorption spectrum [119]. Here the calculations overestimate the observations by 84 cm⁻¹. On the other hand, in deuterated samples, the analogous peak was observed at 1449 cm⁻¹ [120] and we estimate it at 1480 cm⁻¹ – the underestimation is now 31 cm⁻¹ only, mostly due to the weaker anharmonicity of the heavier oscillator (the description of the chemical bond in both cases is the same). This effect is well known and abundantly discussed in the literature (see for instance Refs. [121, 122]).

Previous theoretical work regarding the structure and vibrational properties of substitutional boron and BH pairs is also well documented (see for instance Refs. [31, 62, 64]). We recalculated the vibrational modes of these point defects to use them as *markers*, so that we can locate more accurately the frequencies of modes from unexplored BH₂ complexes. For a review on hydrogen and hydrogen-impurity properties in Si, including vibrational properties, see Ref. [5] and references therein.

A substitutional ¹¹B species gives rise to a well-known vibrational peak at 620 cm⁻¹, corresponding to a degenerate triplet state involving vibrations of B against its Si neighbors along all three (100) directions. We refer to these as B-Si bond stretching modes and they are calculated at 621 cm⁻¹. Such an agreement suggests that the anharmonicity is comparable to the softening effect from the limitations in the exchange correlation description. Additionally, and according to the above, calculations of comparable B-Si vibrations from other defects should also display a similar vanishing error. Tab. III clearly shows that the highest-frequency B-related mode of the BH pair, calculated at 657 cm⁻¹ matches well the ex-

Table III. Calculated local vibrational mode frequencies ($v_{\rm calc}$ in cm⁻¹), their oscillator strengths (f in |e| units where e is the electron charge), symmetry representation within the respective point group of symmetry, and bond localization, where "str" and "wag" stand for stretching and wagging modes, respectively. Symmetry point groups are T_d (B⁻), D_{3d} (H⁺, D⁺), C_{3v} (BH and BH₂⁻) and C_{2v} (BH₂⁺). Some experimental vibrational frequencies ($v_{\rm exp}$ in cm⁻¹) and respective references are also included. Calculated frequencies involving boron defects used the mass of the most abundant ¹¹B isotope.

Defect	$v_{ m calc}$	f	Sym.	$v_{ m exp}$	Localization
$\overline{\mathrm{H}^{+}}$	2082	18.73	a_{2u}	1998 [119]	Si-H ⁺ -Si (str)
D^{+}	1480	12.72	a_{2u}	1449 [1 <mark>20</mark>]	Si-D ⁺ -Si (str)
B-	621	0.22	t_2	620 [<mark>61</mark>]	B-Si (str)
ВН	2027	19.23	a_1	1903 [94]	$Si-H_{BC}\cdots B$ (str)
	657	0.07	e	652 [<mark>61</mark>]	B-Si (str)
	537	0.01	a_1		B-Si (str)
$BH_2^-(A)$	2265	3.15	a_1		$B-H_{BC}\cdots Si$ (str)
	1788	1.90	a_1		Si-H _{AB} (str)
	769	1.01	e		Si-H _{AB} (wag)
	707	~ 0	e		B-H _{BC} (wag)
	604	0.10	e		B-Si (str)
4.15					
$BH_2^-(A')$	2175	5.45	a_1		$B-H_{AB}$ (str)
	2087	1.10	a_1		$Si-H_{BC}\cdots B$ (str)
	860	0.95	e		B-H _{AB} (wag)
	680	0.20	e		B-Si (str)
	561	0.52	e		Si-H _{BC} (wag)
DII±(D)	2106	12.00			C: II
$BH_2^+(D)$	2186	13.98	a_1		$Si-H_{BC}\cdots B$ (str)
	2075	23.48	b_1		$Si-H_{BC}\cdots B$ (str)
	718	1.23	b_2		B-Si (str)
	688	0.32	b_1		Si-H _{BC} (wag)
	544	2.43	a_1		Si-H _{BC} (wag)

perimental counterpart observed at 652 cm⁻¹[61]. This is a doublet involving B oscillations in the plane perpendicular to the Si-H···B axis, and results from the $t_2 \rightarrow e + a_1$ unfolding of the substitutional B mode, due to the presence of H. The singlet state (a_1) is calculated at 537 cm⁻¹, very close to 515 cm⁻¹, which was the calculated highest frequency of a pristine silicon supercell.

The BH complex also gives rise to a well-known stretching vibration localized on the Si-H \cdots B structure, leading to an infra-red absorption band at 1903 cm $^{-1}$ [40, 52, 53, 61, 94]). Previous calculations slightly underestimated this frequency, pointing to values in the range 1830-1880 cm $^{-1}$ [31, 62]. We can only explain such nice agreement if we allow for some error bars (*e.g.* due to limitations in the description of the electronic structure or boundary conditions) That frequency is here predicted at 2027 cm $^{-1}$. It sets our overestimation to

124 cm⁻¹ for this type of mode, allowing us to better estimate similar modes for BH₂ complexes.

All three structures of BH₂ (D, A and A') give rise to three stretching modes plus two wagging modes (Tab. III). However, the modes are all non-degenerate for BH₂⁺, in contrast to both BH₂⁻ complexes, where three of the modes are doubly degenerate. BH₂⁻(A) and BH₂⁻(A') complexes form Si-H_{BC} \cdots B-H_{AB} and B-H_{BC} \cdots Si-H_{AB} pairs, each having two H-related stretching vibrations, two H-related wagging vibrations, and one B-related stretching vibration. The BH₂⁺(D) complex also has two stretching modes and two wagging modes localized on two equivalent Si-H units. Unlike for the acceptor states, where Si-H and B-H oscillators are rather independent, H-modes in BH₂⁺(D) are strongly coupled and form symmetric and asymmetry pairs.

Among the BH_2 complexes, $BH_2^-(A')$ and $BH_2^+(D)$ possess modes localized on $Si-H_{BC}$ units, which are of the same type of the BH-pair stretching mode. For the acceptor, it has a frequency of 2087 cm⁻¹ and it is mostly localized on the $Si-H_{BC}$ bond. Hence, after being subject to the correction of 124 cm^{-1} , this mode is anticipated at 1963 cm^{-1} . The donor state, on the other hand, has symmetric and anti-symmetric modes on a $Si-H\cdots B\cdots H-Si$ structure. They are calculated at 2186 and 2075 cm^{-1} , meaning that our best estimate for these frequencies (after the correction) becomes 2062 and 1951 cm^{-1} , respectively.

So far, we could only find the work of Fukata *et al.* [123] suggesting the formation of complexes with direct B-H bonds. The measurements were performed in plasma-hydrogenated B-implanted n-type Si, where several infra-red absorption bands in the range 2280-2470 cm $^{-1}$ were attributed to B-H vibrations. One of the bands could be related to the most stable acceptor form of BH $_2$ with calculated B-H stretching frequencies of 2265 cm $^{-1}$. Interestingly, the formation of B-H related complexes/clusters was accompanied by an increase in resistivity of the samples. Compensation by BH $_2^-$ (A) complexes in the n-type samples could contribute to this effect.

From a theoretical perspective, we highlight that the two Si-H stretching modes of $BH_2^+(D)$ are predicted to have a strong oscillator strength. Of course, a small concentration of such complexes available in the Si may prevent their detection.

We end with a final note regarding the bonding of the BH pair. Analysis of the isotope shifts can provide us with evidence that H is chemically connected to Si (and not to B). Let us approximate the pair to an oscillating X-H bond, X being either B or Si, with frequency v and a spring constant that is independent of the masses m_X and m_{Si} . If species X is replaced by a lighter element X' with mass $m_{X'}$ the frequency is enhanced by $\Delta v = v(\sqrt{\mu/\mu'} - 1)$, where μ and μ' are reduced masses of X-H and X'-H pairs, respectively. Now, if X is a boron atom, for an oscillating frequency of $v=1900~{\rm cm^{-1}}$ we obtain $\Delta v\approx 8~{\rm cm^{-1}}$ upon replacing $X=^{11}{\rm B}$ by $X'=^{10}{\rm B}$ (boron natural isotopes with respective abundance of 80% and 20%). Instead, from the first-principles calculations we obtain a frequency shift smaller than 2 cm⁻¹ for such substitution in the BH pair, suggesting that the coupling between H and B atoms is much weaker than that for a direct B-H bond. This result is supported by infra-red absorption data, which show a minor shift in the BH band of nearly 1 cm⁻¹ after comparing floating-zone samples implanted either with ¹¹B or ¹⁰B ions [124, 125].

If on the other hand, we assume that X is a silicon atom, the harmonic dimer model gives $\Delta v \approx 2~{\rm cm}^{-1}$ upon replacing $X=^{30}$ Si by $X'=^{28}$ Si , and that matches the analogous quantity that was calculated from first-principles for the replacement of the Si atom in the Si-H···B structure.

IV. DISCUSSION AND CONCLUSIONS

We presented a comprehensive set of first-principles calculations regarding the properties of acceptor-hydrogen complexes in silicon, including electronic transition energies, local vibrational modes and respective intensities, defect-crystal strain coupling and electron localization function. Reactions involving atomic and molecular hydrogen with the acceptors were also investigated. From the calculated reaction barriers, the change of free energy, and the charge state dependence of these quantities, we provided a finite-temperature account of thermally-activated and carrier-capture-activated processes involving acceptor-hydrogen complexes in p-type Si.

The electronic structure of the BH pair was investigated as a function of the distance between B and H units. Electric charges of infinitely separated B^- and H^+ pairs are mutually compensated. An electron trap due to isolated H (donor transition) was estimated at $E_c - 0.19$ eV. As the B-H distance decreases, the H electron trap and the B hole trap are increasingly affected by repulsive potentials, and as a result, they approach the band edges. The electron trap due to third neighboring B-H pairs is estimated to be 20 meV below the conduction band bottom. Second neighbor pairs already show a clean gap. Finally, the ground state of BH shows a true chemical passivation. As proposed nearly three decades ago [52] – it comprises a covalently connected, fully saturated \equiv Si-H···B \equiv structure, where Si, B and H are four-fold, three-fold and mono coordinated, respectively.

The above picture is essentially identical for pairs involving heavier group-III species (X). From the electron localization function analysis, we found that the ground state of all XH pairs also comprise fully saturated $\equiv \text{Si-H} \cdots X \equiv \text{structures}$. The three-atom structure is linear for BH, whereas it is puckered for other XH pairs with the Si-H bond making an angle of about 20° away from the $\langle 111 \rangle$ direction.

Motion of H in the $\{111\}$ plane, via oscillations for the case of BH, or rotation of the Si-H bond around $\langle 111 \rangle$ for other XH pairs, is found to be governed by a very flat potential energy landscape with variations of a few meV. This picture is compatible with the model of Stavola *et al.* [93, 94], which describes the vibrational activity of the pairs as arising from the coupling between a low-frequency degree of freedom (with tens of cm⁻¹ involving atomic motion perpendicular to $\langle 111 \rangle$), and a high-frequency stretching mode of the Si-H unit.

There are two main sources of error that affect the calculated frequencies: neglected anharmonic regions of the potential energy surface, and inherent insufficiencies in the electronic structure method for its evaluation. High frequencies

with well defined potential valleys can be easily corrected by ad-hoc shifts or scaling factors [117]. A more elaborate method involves the extraction of anharmonic frequencies directly from atomic trajectory data of first-principles molecular dynamics at finite temperatures [126]. On the other hand, the low-frequency rotational motion of XH (and its coupling to the Si-H stretching mode) belongs to a class of extreme cases, involving a shallow potential with several minima, where the error bar of first-principles electronic structure calculations overlaps many times the potential variations and the separation between the rotovibrational levels. Further progress in the understanding the low-frequency motion of BH could however be attained by construction of the potential, partially by first-principles and fitting to experimental data, and solving the anharmonic Schrödinger equation. This approach has been successful in the description of the rotovibrational motion of bond centered interstitial oxygen in Si [96–98].

The calculated binding energies and dissociation barriers of XH pairs are respectively in the range 0.76-0.95 eV and 1.18-1.37 eV. They depend weakly on the acceptor species, with BH showing the smallest figures and GaH showing an off-trend deviation with increasing the mass of the acceptors. These features were previously observed [60] and are now theoretically accounted for. We demonstrate that size/strain effects are not essential to explain the observed trends. Instead, they are justified based on the relatively stronger B-Si bond (that has to be broken before formation of the BH pair), and the d-block contraction of the gallium species.

Ground state XH pairs do not interact with minority carriers in p-type Si. However, if X^- and H^+ become separated by several Si-Si bonds, the hydrogen atom could trap electrons, and that is found to decrease the dissociation energy in two manners: (1) via reaction X^- - H^+ + $e^- \rightarrow X^-$ + H^0 , which lowers E_d by of up to 0.17 eV in comparison to an electron deprived dissociation; (2) due to the accelerated migration of H^0 . The complex migration of H^0 makes the latter effect more difficult to be quantified [91]. Both effects are invoked to play a role in the enhanced injection-/photo-induced dissociation of BH pairs by slowing the rate of the back reaction $XB \leftarrow X^- + H^+$ against that of the forward reaction during annealing treatments.

For the specific case of BH, the dissociation enhancement upon electron trapping is likely to be limited by the relatively large barrier for breaking the pair (before it can trap electrons), $E_{\rm d1}\approx 1$ eV. This translates into a decrease of the dissociation energy by about 0.2 eV when compared to the same property without electron trapping. For other acceptor-hydrogen pairs on the other hand, the barrier for the first H jump is lower, the dissociation energy is now limited by $E_{\rm d}^*=E_{\rm b}^*+E_{\rm m}^*$ (see Fig. 2), and the effect of electron trapping is expected to be even more conspicuous due to the fast escape of H⁰. In the extreme case of a negligible $E_{\rm m}^*$, we would have $E_{\rm d}^*\geq 0.8$ eV for the heavier XH pairs.

In Ref. [28] it was postulated that regeneration of BO-LID-degraded solar Si results from the transfer of H from BH pairs to boron-dioxygen LID defects, effectively passivating the latter and leading to a slightly more stable BO₂-H complex. Our results indicate that the role of light in that process is to intro-

duce a population of electrons that promote a carrier-induced destabilization of BH pairs in favor of more stable (and perhaps less light-sensitive) BO₂-H complexes.

From the calculation of the free energy change across the reaction $B^- + H^+ \rightleftharpoons BH$, we estimated the annealing temperature of BH in the dark at about 180 °C. This figure considered a boron concentration $[B] \sim 10^{15}~\text{cm}^{-3}$. The process is dominated by the larger configurational entropy of the reactants, and due to its dependence on [B], the annealing temperature shows some variation (tens of degrees Celsius). We did not find any significant impact of the hydrogen mass to the free energy change of the reaction, and therefore to the annealing temperature. Note that this conclusion refers to an equilibrium property, and it is not contradictory with different dissociation rates of BH and BD due to comparably more frequent H jumps.

The interaction of H₂ molecules with the acceptors, interstitial oxygen and substitutional carbon was also investigated. In monocrystalline p-type Si wafers, oxygen and carbon are abundant impurities and along with the acceptors, they compete for trapping the molecules. In general, for remote impurity-H₂ pairs (separation $r \gtrsim 10 \text{ Å}$) strain interactions result in an energy change within ± 10 meV only. Significant differences become noticeable only for $r \leq 5$ Å, where the magnitude of the potentials becomes larger than k_BT at room temperature. Interstitial oxygen was found to be the most attractive center for the formation of impurity-H2 pairs (without molecular dissociation). The calculated binding energy of adjacent O-H₂ pairs exceeds 0.2 eV. Carbon is the most repulsive impurity. Boron was also found to be repulsive for the molecules, whereas larger acceptors are slightly attractive. These effects are well accounted for by the relative volume that is available for H₂ in the vicinity of the several impurities. Essentially, compressive (O, Ga, Al, In) and tensile (C and B) defects, respectively increase and reduce the volume of their first neighboring tetrahedral interstitial sites. Hence, they respectively attract and repel the molecules before any intimate reaction takes place.

The chemical reaction of H₂ molecules with boron, and subsequent molecular dissociation, was found to involve the collision of H₂ with a first neighboring B-Si bond. An activation energy of 1.1 eV was found for this process. This barrier is considerably lower than the 1.62 eV which was previously estimated for H₂ dissociation in pristine bulk Si [91], but also larger than the barrier for H₂ migration (0.78 eV [37, 39]). These findings offer an alternative explanation for H₂ dissociation in B-doped Si without the involvement of holes, as proposed in Ref. [41] for the first step of reaction 1 described in the Introduction. We also found that immediately after the saddle point for H₂ dissociation next to B, a metastable structure involving H⁻ next to BH is attained. From here, hole capture and reconfiguration events are likely to influence the final result, which could be formation of BH₂, BH₂ or BH pairs.

An analogous study was carried out for the dissociation of H_2 next to carbon impurities. The height of the barrier for $C+H_2 \rightarrow CH_2$ was found to be $E_d=1.35$ eV. This suggests that C is also a catalyst for H_2 dissociation in Si, although

perhaps less effective than boron. Along the reaction, an intermediate stable structure made of close $C\text{-}H\cdots H\text{-}Si$ bonds was found. However, this state is electrically inactive, therefore the participation of carriers is unlikely to occur during further transformations toward the lowest energy CH_2 structures.

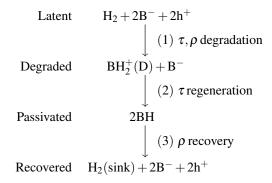
The most favorable products from the reaction of H_2 with B and C are BH pairs and CH_2 complexes, respectively. These correspond to respective potential energy drops of 1.19 eV and 0.91 eV per molecule. After considering finite temperature effects, the free energy drop across $H_2 + 2B^- + 2h^+ \rightarrow 2BH$ was found to be still invariably larger than that for $H_2 + C \rightarrow CH_2$. From these results and the calculated reaction barriers, we conclude that during the cooling of Si that has been in contact with a hot hydrogen source, interstitial H_2 molecules are more likely to react with boron than carbon, unless the concentration of the latter is dominant.

The results point toward a strong thermodynamic drive for dispersion of H in the form of BH pairs in B-doped Si. Dihydrogenated boron is a by-product along the $2B^- + H_2 +$ $2h^+ \rightarrow 2BH$ reaction. BH_2 in Si is a negative-U defect with a metastable neutral state. The (-/+) transition is anticipated at $E(-/+) - E_v = 0.26$ eV and involves different geometries for the donor and acceptor states. The positive charge state has two Si-H bonds next to undercoordinated boron, giving rise to an electron trap with an energy level at $E_c - 0.19$ eV. The negative charge state has a four-fold coordinated boron atom and is responsible for a shallow acceptor level close to that of isolated boron. As for heavier acceptor-H₂ complexes involving Al, Ga and In, they mainly differ from BH₂ in that the donor states are shallow effective-mass-like. As a corollary, besides the subtraction of one hole, formation of heavier XH_2^+ complexes lead to donation of one electron as well.

BH $_2^+$ and BH $_2^-$ are not very stable complexes. The acceptor is not even stable above $T\sim 100~\rm K$ against B $^-+H_2$ in p-type Si. As for the donor state, it becomes less stable than B $^-+2H^+$ at $T\gtrsim 300~\rm K$ and the activation energy for dissociation of a proton is about 0.8 eV. These results, along with the calculated donor transition of BH $_2$ at $E_c-0.19$ eV, indicate that BH $_2$ is effectively a donor defect (without a stable acceptor) in the range $T\approx 100\text{--}300~\rm K$. They also support the assignment of this defect to the experimentally detected electron trap at $E_c-0.175~\rm eV$, which was found to anneal out at 280 K, and was connected to the LeTID of solar cells based on B-doped Si [59].

From the calculated local vibrational mode frequencies of boron-hydrogen defects, including B- and H-related isotope shifts, we confirm the structure of the BH pairs, and in particular the chemical passivation model, according to which a Si-H covalent bond is established. We have also calculated the frequency and relative intensity of several vibrational modes of BH₂ complexes. These results are expected to provide guidance for future experiments toward a better identification of these centers.

Finally, regarding the LeTID of boron-doped Si solar cells, and in the light of our results, we recall the sequence of reactions proposed by de Guzman *et al.* [59] for the degradation and recovery steps under dark annealing conditions,



The above reaction sequence adds a *Degraded* state to the three-state-model of Voronkov and Falster [41] (see Eq. 1), which has been used to explain changes in resistivity of hydrogenated boron doped Si crystals during heat/illumination treatments. We refer to the three states of the original model as Latent, Passivated and Recovered. LeTID initiates from a Latent state, where H₂ molecules linger in the as-fired/quenched devices. Lifetime (τ) degradation occurs during step (1) when heat is provided, and H₂ is able to escape from trapping sites, most notably O impurities, and react with B to form BH2. We note that already at this stage, for each BH₂⁺ complex that is formed, two free-holes are subtracted. This means that the resistivity (ρ) change and lifetime degradation are concurrent, and any measured resistivity increase rate, also reflects the lifetime degradation rate. The calculated activation energy for step (1) is 1.1 eV and corresponds to the dissociation of H₂ next to B. This quantity compares well with the LeTID activation energy of 1.08 eV from the study of Vargas et al. [35].

The recovery of lifetime and resistivity occur separately. Lifetime regeneration involves the annealing of $BH_2^+(D)$ and formation of BH pairs in step (2) According to our calculations, the activation energy for $BH_2^+(D) \to BH + H^+$ is 0.8 eV and the proton should be captured by another boron atom. Importantly, step (2) does not involve a change in the free-hole concentration, but rather attaining a passivated state with a weak recombination activity.

Following Refs. [41, 45], one may speculate that the recovery of resistivity upon prolonged dark annealings, involves the dissociation of BH pairs and subsequent trapping of hydrogen at some kind of sink. This would explain the full recovery of the devices and reactivation of the B dopants as described by step (3). The calculated dissociation barrier of BH (1.2 eV) is close to the measured counterpart (1.28 eV [60]) and also close to the activation energy for the recovery of resistivity (1.1-1.3 eV [35, 44, 49]).

Appendix A: Configurational entropy for $B^- + H^+ \rightarrow BH$

For the evaluation of configurational entropy, we have to estimate the total number of equivalent microstates in the reactants and products sides of the reaction of interest, W_R and W_P , respectively. This is only tractable upon consideration of a few assumptions.

Firstly, we consider a crystalline sample made of $n_{\rm Si}$ silicon sites, containing $n_{\rm B}$ substitutional boron acceptors and $n_{\rm H}$ hydrogen atoms subject to $n_{\rm Si} \gg n_{\rm B} \gg n_{\rm H}$;

Next, because hydrogen is a fast diffuser and boron is strongly *anchored* to the lattice, at low temperatures all hydrogen is inferred to be trapped by boron (in the form of BH pairs), so that the number of pairs is also $n_{\rm H}$. The remaining boron is electrically activated;

At high temperatures, all pairs dissociate into uncorrelated B⁻ and H⁺ elements. The number of free carriers is conserved along the process and no change of electronic entropy is considered;

Finally, at low temperatures, BH pairing is only considered to occur upon formation of first neighboring complexes. Any other configurations are, for the sake of the calculation of configurational entropy, equivalent to isolated B⁻ and H⁺ species.

The relevant reaction is therefore,

$$n_{\rm B}B^- + n_{\rm H}H^+ \to (n_{\rm B} - n_{\rm H})B^- + n_{\rm H}BH.$$
 (A1)

When all BH are dissociated, the number of microstates for the reactants side is found by first distributing the $n_{\rm B}$ acceptors (there are $n_{\rm Si}!/(n_{\rm Si}-n_{\rm B})!n_{\rm B}!$ ways to do that), and for each boron-related microstate we distribute the $n_{\rm H}$ hydrogen atoms among the available $2n_{\rm Si}-4n_{\rm B}$ bond center sites not adjacent to boron. The total number of ways to perform the two operations is,

$$W_{\rm R} = \frac{n_{\rm Si}!}{(n_{\rm Si} - n_{\rm B})! n_{\rm B}!} \times \frac{(2n_{\rm Si} - 4n_{\rm B})!}{(2n_{\rm Si} - 4n_{\rm B} - n_{\rm H})! n_{\rm H}!}.$$
 (A2)

On the other hand, when all H is trapped by boron, the total number of possible microstates for the products side is given by the number of ways to distribute the $n_{\rm B}$ boron atoms times the number of ways to distribute $n_{\rm H}$ hydrogen atoms on $4n_{\rm B}$ bond centered sites next to boron,

$$W_{\rm P} = \frac{n_{\rm Si}!}{(n_{\rm Si} - n_{\rm B})! n_{\rm B}!} \times \frac{(4n_{\rm B})!}{(4n_{\rm B} - n_{\rm H})! n_{\rm H}!}.$$
 (A3)

Using Stirling's approximation, we find that the total entropy change is linear with $n_{\rm H}$, and we may derive the change of configurational entropy per BH pair as,

$$\Delta S_{\text{conf}} = \frac{k_{\text{B}}}{n_{\text{H}}} \ln \left(\frac{W_{\text{P}}}{W_{\text{R}}} \right) = k_{\text{B}} \ln(2c_{\text{B}}), \tag{A4}$$

where $k_{\rm B}$ is the Boltzmann constant and $c_{\rm B} = n_{\rm B}/n_{\rm Si}$ is the fractional concentration of boron. If we were to consider up to second neighboring bonds to distinguish between pairing formation/dissociation, the factor of 2 next to $c_{\rm B}$ would have to be replaced by 8, thus having a minute impact on the final result.

Appendix B: Configurational entropy for $B^- + \frac{1}{2}H_2 + h^+ \to BH$

Now we implicitly assume that multi-trapping of H at B is negligible, so that the number of resulting pairs is also $n_{\rm H}$, and that after the reaction, the remaining $(n_{\rm B}-n_{\rm H})$ boron ions are ionized. Again, taking $n_{\rm Si}\gg n_{\rm B}\gg n_{\rm H}$, the relevant reaction is.

$$n_{\rm B}({\rm B}^- + {\rm h}^+) + \frac{n_{\rm H}}{2}{\rm H}_2 \rightarrow (n_{\rm B} - n_{\rm H})({\rm B}^- + {\rm h}^+) + n_{\rm H}{\rm BH}, \ ({\rm B}1)$$

which highlights the fact that each hydrogen molecule is capable of subtracting two holes from the sample. Since the number of free holes is not conserved across reaction B1, the effect of electronic entropy should be assessed as well. In this appendix we evaluate the configurational term.

For the reactants side, we assume that the $n_{\rm B}$ boron ions and the $n_{\rm H}/2$ molecules are perfectly uncorrelated, and they can occupy any of the $n_{\rm Si}$ substitutional and $n_{\rm Si}$ tetrahedral interstitial sites, respectively. The number of ways to distribute such populations is

$$W_{\rm R} = \frac{n_{\rm Si}!}{(n_{\rm Si} - n_{\rm B})! n_{\rm B}!} \times \frac{2^{n_{\rm H}/2} n_{\rm Si}!}{(n_{\rm Si} - n_{\rm H}/2)! (n_{\rm H}/2)!},$$
 (B2)

where the factor of $2^{n_{\rm H}/2}$ accounts for the two possibilities that we have to form each molecule.

As for the number of microstates in the products side (W_P) we can use Eq. A3 from Appendix A. Hence, the configurational entropy change per BH pair can be approximated to

$$\Delta S_{\text{conf}} = \frac{k_{\text{B}}}{n_{\text{H}}} \ln \left(\frac{W_{\text{P}}}{W_{\text{R}}} \right) = \frac{k_{\text{B}}}{2} \left[\ln \left(\frac{8c_{\text{B}}^2}{c_{\text{H}}} \right) + 1 \right], \quad (B3)$$

where $c_{\rm B} = n_{\rm B}/n_{\rm Si}$ and $c_{\rm H} = n_{\rm H}/n_{\rm Si}$ are the fractional concentrations of boron and hydrogen, respectively.

Appendix C: Configurational entropy for $C + H_2 \rightarrow CH_2$

It is known that CH pairs are not very stable. They dissociate at $T \sim 100$ °C in darkness and even below 230 K upon illumination with above band gap light [127]. Therefore, we assume that interactions between H₂ and C upon quenching from H₂ exposure at high temperatures, essentially lead to formation of CH₂ complexes [110].

Again, taking $n_{\rm Si} \gg n_{\rm C} \gg n_{\rm H}$, where $n_{\rm C}$ is the number of substitutional carbon impurities in the sample, and the number of resulting CH₂ complexes as $n_{\rm H}/2$, the relevant reaction is,

$$n_{\rm C}C + (n_{\rm H}/2)H_2 \rightarrow (n_{\rm C} - n_{\rm H}/2)C + (n_{\rm H}/2)CH_2,$$
 (C1)

On the reactants side, we have $n_{\rm Si}!/(n_{\rm Si}-n_{\rm C})!n_{\rm C}!$ ways to distribute the C atoms while H₂ molecules can occupy tetrahedral interstitial sites. Considering also that there are two

ways to form each molecule (see Eq. B2), the total number of microstates becomes,

$$W_{\rm R} = \frac{n_{\rm Si}!}{(n_{\rm Si} - n_{\rm C})!n_{\rm C}!} \times \frac{2^{n_{\rm H}/2} n_{\rm Si}!}{(n_{\rm Si} - n_{\rm H}/2)!(n_{\rm H}/2)!}.$$
 (C2)

Conversely, when all H_2 is trapped at the C atoms, the total number of possible microstates for the products side is now the number of ways to distribute the $n_{\rm C}$ carbon atoms times the number of ways to combine them with the $n_{\rm H}/2$ pairs of H atoms. Considering that each ${\rm CH_2}$ complex has four-fold orientational degeneracy, and again the two possibilities for the formation of each complex (due to the existence of two H atoms), one finds,

$$W_{\rm P} = \frac{n_{\rm Si}!}{(n_{\rm Si} - n_{\rm C})! n_{\rm C}!} \times \frac{2^{n_{\rm H}/2} (4n_{\rm C})!}{(4n_{\rm B} - n_{\rm H}/2)! (n_{\rm H}/2)!}.$$
 (C3)

Following the same procedure as in Appendix A and B, we have the configurational entropy change per H atom,

$$\Delta S_{\text{conf}} = \frac{k_{\text{B}}}{2} \ln(4c_{\text{C}}), \qquad (C4)$$

where $c_{\rm C} = n_{\rm C}/n_{\rm Si}$ is the fractional concentrations carbon.

Appendix D: Electronic free energy

For solid state reactions where there is a variation in the number of free carriers, the contribution of electronic entropy to the free energy change can be comparable to other terms. This is particularly relevant when we are dealing with reactions that involve the thermal promotion of carriers, such as $D^0 \to A^- + h^+,$ where D is a deep or electronically inactive defect, while A stands for an arbitrary shallow acceptor, and h^+ a free hole in thermal equilibrium with the sample.

We restrict our analysis to the low doping regime at room temperature and up to few hundred Kelvin (LeTID conditions), where virtually all shallow acceptors (boron or BH₂(A) complexes) are ionized. At these temperatures, intrinsic excitations are negligible and that is reflected in the excellent agreement between the calculated specific heat, obtained from vibrational degrees of freedom only, and the measurements [86, 91]. For low doping conditions, the effective density of valence band states largely exceeds the free hole concentration $(N_v \gg p)$ and we can apply Boltzmann statistics. For instance, for the reaction

$$B^- + \frac{1}{2}H_2 + h^+ \to BH,$$
 (D1)

the electronic free energy change is estimated from that of a free-hole gas with density $\Delta p = f c_{\rm H} [{\rm Si}]$, where $f = \exp(-E_{\rm h}/k_{\rm B}T)$ is the Boltzmann distribution function, and $E_{\rm h}$ the hole binding energy to the acceptor ($E_{\rm h} = 46$ meV for the boron acceptor [77]).

In the classical limit, and as proposed by Estreicher *et al.* [86], the electronic free energy change due to thermal release of a hole from a shallow state into the electronic thermal bath of the sample, is given by [128]

$$\Delta F_{\text{elec,h}} = f(\mu - k_{\text{B}}T), \tag{D2}$$

where μ is the electronic chemical potential with respect to the valence band top. Equation D2 finds the Helmholtz free energy by simply subtracting pV (which is k_BT for a classical gas of non-interacting holes) to the Gibbs free per hole (μ) .

The chemical potential is approximated to $\mu = k_{\rm B}T\ln(\Delta p/N_{\rm v})$, where $N_{\rm v}$ is obtained numerically in the range $T=200\text{-}500~{\rm K}$ as $N_{\rm v}=3.10\times10^{19}(T/300)^{1.85}~{\rm cm}^{-3}$ [129]. For the temperatures of interest, i.e., $T\approx300\text{-}500~{\rm K}$, we have $f\approx1$ and provided that $\Delta p\ll p\ll N_{\rm v}$, equation D2 allows us to estimate the electronic free energy variation due to small increase of free holes, across a reaction that involves the full ionization/passivation of shallow acceptors.

ACKNOWLEDGMENTS

We acknowledge the FCT through projects LA/P/0037/2020, UIDB/50025/2020, UIDP/50025/2020 and 2021.09643.CPCA (Advanced Computing Project using the Oblivion supercomputer). The work in the UK was funded by EPSRC via grant EP/TO25131/1.

^[1] M. Stutzmann and C. P. Herrero, Physica Scripta **T25**, 276 (1989).

^[2] J. I. Pankove and N. M. Johnson, eds., *Hydrogen in Semiconductors*, Semiconductors and Semimetals, Vol. 34 (Academic Press, Boston, 1991).

^[3] S. J. Pearton, J. W. Corbett, and M. Stavola, *Hydrogen in Crystalline Semiconductors*, edited by H.-J. Queisser, Springer Series in Materials Science, Vol. 16 (Springer-Verlag, Berlin, 1992)

^[4] N. Nickel, ed., Hydrogen in Semiconductors II, Semiconduc-

tors and semimetals, Vol. 61 (Academic Press, San Diego, 1999).

^[5] S. K. Estreicher, M. Stavola, and J. Weber, Silicon, Germanium, and their Alloys: Growth, Defects, Impurities, and Nanocrystals (CRC Press, Boca Raton, 2014) Chap. 7, pp. 217–254.

^[6] J. I. Pankove, D. E. Carlson, J. E. Berkeyheiser, and R. O. Wance, Physical Review Letters **51**, 2224 (1983).

^[7] S. J. Pearton, J. W. Corbett, and T. S. Shi, Applied Physics A Solids and Surfaces 43, 153 (1987).

- [8] J. Mullins, S. Leonard, V. P. Markevich, I. D. Hawkins, P. Santos, J. Coutinho, A. G. Marinopoulos, J. D. Murphy, M. P. Halsall, and A. R. Peaker, physica status solidi (a) 214, 1700304 (2017).
- [9] C. H. Seager, Annual Review of Materials Science 15, 271 (1985).
- [10] B. L. Sopori, X. Deng, J. P. Benner, A. Rohatgi, P. Sana, S. K. Estreicher, Y. K. Park, and M. A. Roberson, Solar Energy Materials and Solar Cells 41-42, 159 (1996).
- [11] A. G. Aberle, Progress in Photovoltaics: Research and Applications 8, 473 (2000).
- [12] P. Deák, L. C. Snyder, and J. W. Corbett, Physical Review B 37, 6887 (1988).
- [13] C. G. V. de Walle, P. J. H. Denteneer, Y. Bar-Yam, and S. T. Pantelides, Physical Review B 39, 10791 (1989).
- [14] T. Sasaki and H. Katayama-Yoshida, Journal of the Physical Society of Japan 58, 1685 (1989).
- [15] R. Jones, Physica B: Condensed Matter 170, 181 (1991).
- [16] C. Herring, N. M. Johnson, and C. G. Van de Walle, Physical Review B 64, 125209 (2001).
- [17] S. K. Estreicher, A. Docaj, M. B. Bebek, D. J. Backlund, and M. Stavola, physica status solidi (a) 209, 1872 (2012).
- [18] N. M. Johnson, C. Herring, and C. G. Van de Walle, Physical Review Letters 73, 130 (1994).
- [19] N. Johnson, C. Herring, and C. V. de Walle, Physical Review Letters 74, 1889 (1995).
- [20] K. B. Nielsen, L. Dobaczewski, S. Søgård, and B. B. Nielsen, Physical Review B 65, 075205 (2002).
- [21] F. Jiang, M. Stavola, A. Rohatgi, D. Kim, J. Holt, H. Atwater, and J. Kalejs, Applied Physics Letters 83, 931 (2003).
- [22] M. Sheoran, D. S. Kim, A. Rohatgi, H. F. W. Dekkers, G. Beaucarne, M. Young, and S. Asher, Applied Physics Letters 92, 172107 (2008).
- [23] A. Herguth, G. Schubert, M. Kaes, and G. Hahn, Progress in Photovoltaics: Research and Applications 16, 135 (2008).
- [24] S. Wilking, A. Herguth, and G. Hahn, Journal of Applied Physics 113, 194503 (2013).
- [25] L. Helmich, D. C. Walter, R. Falster, V. V. Voronkov, and J. Schmidt, Solar Energy Materials and Solar Cells 232, 111340 (2021).
- [26] J. Schmidt and K. Bothe, Physical Review B 69, 024107 (2004).
- [27] T. Niewelt, J. Schon, W. Warta, S. W. Glunz, and M. C. Schubert, IEEE Journal of Photovoltaics 7, 383 (2017).
- [28] T. O. A. Fattah, V. P. Markevich, J. A. T. D. Guzman, J. Coutinho, S. B. Lastovskii, I. D. Hawkins, I. F. Crowe, M. P. Halsall, and A. R. Peaker, physica status solidi (a) 219, 2200176 (2022).
- [29] C.-T. Sah, J. Y.-C. Sun, and J. J.-T. Tzou, Applied Physics Letters 43, 204 (1983).
- [30] N. M. Johnson, C. Herring, and D. J. Chadi, Physical Review Letters 56, 769 (1986).
- [31] P. J. H. Denteneer, C. G. V. de Walle, and S. T. Pantelides, Physical Review B 39, 10809 (1989).
- [32] S. K. Estreicher, C. H. Seager, and R. A. Anderson, Applied Physics Letters **59**, 1773 (1991).
- [33] K. Ramspeck, S. Zimmermann, H. Nagel, A. Metz, Y. Gassenbauer, B. Birkmann, and A. Seidl, in *Proceedings of the 27th European Photovoltaic Solar Energy Conference and Exhibition* (WIP, Munich, 2012) pp. 861–865.
- [34] D. Bredemeier, D. C. Walter, R. Heller, and J. Schmidt, physica status solidi (RRL) Rapid Research Letters 13, 1900201 (2019).
- [35] C. Vargas, G. Coletti, C. Chan, D. Payne, and Z. Hameiri, So-

- lar Energy Materials and Solar Cells 189, 166 (2019).
- [36] D. Chen, M. V. Contreras, A. Ciesla, P. Hamer, B. Hallam, M. Abbott, and C. Chan, Progress in Photovoltaics: Research and Applications 29, 1180 (2020).
- [37] R. E. Pritchard, M. J. Ashwin, J. H. Tucker, and R. C. Newman, Physical Review B 57, R15048 (1998).
- [38] R. E. Pritchard, J. H. Tucker, R. C. Newman, and E. C. Lightowlers, Semiconductor Science and Technology 14, 77 (1999).
- [39] V. P. Markevich and M. Suezawa, Journal of Applied Physics 83, 2988 (1998).
- [40] P. M. Weiser, E. Monakhov, H. Haug, M. S. Wiig, and R. Søn-denå, Journal of Applied Physics 127, 065703 (2020).
- [41] V. V. Voronkov and R. Falster, physica status solidi (b) 254, 1600779 (2017).
- [42] D. C. Walter, D. Bredemeier, R. Falster, V. V. Voronkov, and J. Schmidt, Solar Energy Materials and Solar Cells 200, 109970 (2019).
- [43] T. H. Fung, M. Kim, D. Chen, A. Samadi, C. E. Chan, B. J. Hallam, S. Wenham, and M. Abbott, in *SiliconPV 2018, the 8th International Conference on Crystalline Silicon Photovoltaics*, AIP Conference Proceedings, Vol. 1999, edited by C. Ballif, R. Brendel, S. Glunz, G. Hahn, J. Poortmans, P.-J. Ribevron, and A. Weeber (Lausanne, 2018) p. 130004.
- [44] C. Winter, J. Simon, and A. Herguth, physica status solidi (a) **218**, 2100220 (2021).
- [45] D. C. Walter, V. V. Voronkov, R. Falster, D. Bredemeier, and J. Schmidt, Journal of Applied Physics 131, 165702 (2022).
- [46] B. Hammann, N. Assmann, P. M. Weiser, W. Kwapil, T. Niewelt, F. Schindler, R. Sondena, E. V. Monakhov, and M. C. Schubert, IEEE Journal of Photovoltaics 13, 224 (2023).
- [47] W. Kwapil and B. Hammann, Solar RRL 7, 2201107 (2023).
- [48] B. Hammann, L. Rachdi, W. Kwapil, F. Schindler, and M. C. Schubert, physica status solidi (RRL) Rapid Research Letters 15, 2000584 (2021).
- [49] Y. Acker, J. Simon, and A. Herguth, physica status solidi (a) 219, 2200142 (2022).
- [50] N. E. Grant, J. R. Scowcroft, A. I. Pointon, M. Al-Amin, P. P. Altermatt, and J. D. Murphy, Solar Energy Materials and Solar Cells 206, 110299 (2020).
- [51] W. Kwapil, J. Dalke, R. Post, and T. Niewelt, Solar RRL 5, 2100147 (2021).
- [52] J. I. Pankove, P. J. Zanzucchi, C. W. Magee, and G. Lucovsky, Applied Physics Letters 46, 421 (1985).
- [53] N. M. Johnson, Physical Review B **31**, 5525 (1985).
- [54] S. T. Pantelides, Applied Physics Letters 50, 995 (1987).
- [55] M. Stutzmann, Physical Review B 35, 5921 (1987).
- [56] K. J. Chang and D. J. Chadi, Physical Review Letters 60, 1422 (1988).
- [57] L. Korpás, J. W. Corbett, and S. K. Estreicher, Physical Review B 46, 12365 (1992).
- [58] J. T. Borenstein, J. W. Corbett, and S. J. Pearton, Journal of Applied Physics 73, 2751 (1993).
- [59] J. A. T. De Guzman, V. P. Markevich, J. Coutinho, N. V. Abrosimov, M. P. Halsall, and A. R. Peaker, Solar RRL 6, 2100459 (2021).
- [60] T. Zundel and J. Weber, Physical Review B 39, 13549 (1989).
- [61] C. P. Herrero and M. Stutzmann, Physical Review B 38, 12668 (1988).
- [62] G. G. DeLeo and W. B. Fowler, Physical Review B 31, 6861 (1985).
- [63] A. A. Bonapasta, A. Lapiccirella, N. Tomassini, and M. Capizzi, Physical Review B 36, 6228 (1987).
- [64] S. K. Estreicher, L. Throckmorton, and D. S. Marynick, Phys-

- ical Review B 39, 13241 (1989).
- [65] G. Kresse and J. Hafner, Physical Review B 47, 558 (1993).
- [66] G. Kresse and J. Furthmüller, Computational Materials Science 6, 15 (1996).
- [67] G. Kresse and J. Furthmüller, Physical Review B 54, 11169 (1996).
- [68] P. E. Blöchl, Physical Review B 50, 17953 (1994).
- [69] J. Heyd, G. E. Scuseria, and M. Ernzerhof, The Journal of Chemical Physics 118, 8207 (2003).
- [70] A. V. Krukau, O. A. Vydrov, A. F. Izmaylov, and G. E. Scuseria, The Journal of Chemical Physics 125, 224106 (2006).
- [71] J. P. Perdew, K. Burke, and M. Ernzerhof, Physical Review Letters 77, 3865 (1996).
- [72] J. Coutinho, V. P. Markevich, and A. R. Peaker, Journal of Physics: Condensed Matter 32, 323001 (2020).
- [73] C. Freysoldt, J. Neugebauer, and C. G. Van de Walle, Physical Review Letters 102, 016402 (2009).
- [74] H.-P. Komsa, T. T. Rantala, and A. Pasquarello, Physical Review B 86, 045112 (2012).
- [75] A. Resende, R. Jones, S. Öberg, and P. R. Briddon, Physical Review Letters 82, 2111 (1999).
- [76] J. Coutinho, V. J. B. Torres, R. Jones, and P. R. Briddon, Physical Review B 67, 035205 (2003).
- [77] A. K. Ramdas and S. Rodriguez, Reports on Progress in Physics 44, 1297 (1981).
- [78] S. Baroni, S. de Gironcoli, A. D. Corso, and P. Giannozzi, Reviews of Modern Physics 73, 515 (2001).
- [79] P. Brüesch, *Phonons: Theory and Experiments II*, Springer Series in Solid-State Sciences (Springer-Verlag, Berlin, Heidelberg, 1986).
- [80] P. Giannozzi and S. Baroni, The Journal of Chemical Physics 100, 8537 (1994).
- [81] M. Gajdoš, K. Hummer, G. Kresse, J. Furthmüller, and F. Bechstedt, Physical Review B 73, 045112 (2006).
- [82] F. Bruneval, C. Varvenne, J.-P. Crocombette, and E. Clouet, Physical Review B **91**, 024107 (2015).
- [83] J. S. Wróbel, M. R. Zemła, D. Nguyen-Manh, P. Olsson, L. Messina, C. Domain, T. Wejrzanowski, and S. L. Dudarev, Computational Materials Science 194, 110435 (2021).
- [84] A. D. Becke and K. E. Edgecombe, The Journal of Chemical Physics 92, 5397 (1990).
- [85] B. Silvi and A. Savin, Nature 371, 683 (1994).
- [86] S. K. Estreicher, M. Sanati, D. West, and F. Ruymgaart, Physical Review B 70, 125209 (2004).
- [87] S. K. Estreicher, K. Wells, P. A. Fedders, and P. Ordejón, Journal of Physics: Condensed Matter 13, 6271 (2001).
- [88] O. K. Al-Mushadani and R. J. Needs, Physical Review B 68, 235205 (2003).
- [89] D. Murali, M. Posselt, and M. Schiwarth, Physical Review B 92, 064103 (2015).
- [90] X. Zhang, B. Grabowski, T. Hickel, and J. Neugebauer, Computational Materials Science 148, 249 (2018).
- [91] D. Gomes, V. P. Markevich, A. R. Peaker, and J. Coutinho, physica status solidi (b) 259, 2100670 (2022).
- [92] G. Henkelman, B. P. Uberuaga, and H. Jónsson, The Journal of Chemical Physics 113, 9901 (2000).
- [93] M. Stavola, S. J. Pearton, J. Lopata, and W. C. Dautremont-Smith, Applied Physics Letters 50, 1086 (1987).
- [94] M. Stavola, S. J. Pearton, J. Lopata, and W. C. Dautremont-Smith, Physical Review B 37, 8313 (1988).
- [95] M. Suezawa, N. Fukata, M. Saito, and H. Yamada-Kaneta, Physical Review B 65, 075214 (2002).
- [96] H. Yamada-Kaneta, physica status solidi (c) 0, 673 (2003).
- [97] H. Yamada-Kaneta, C. Kaneta, and T. Ogawa, Physical Re-

- view B 42, 9650 (1990).
- [98] K. Laßmann, B. P. Gorshunov, A. S. Prokhorov, E. S. Zhukova, P. S. Korolev, V. P. Kalinushkin, V. G. Plotnichenko, N. V. Abrosimov, P. G. Sennikov, H.-J. Pohl, and M. Dressel, Physical Review B 86, 075201 (2012).
- [99] M. Stavola, K. Bergman, S. J. Pearton, and J. Lopata, Physical Review Letters 61, 2786 (1988).
- [100] G. Marx and R. Vianden, Hyperfine Interactions 97-98, 211 (1996).
- [101] Y.-R. Luo, Comprehensive Handbook of Chemical Bond Energies (CRC Press, Boca Raton, 2007).
- [102] J. B. Mann, Atomic Structure Calculations II. Hartree-Fock Wavefunctions and Radial Expectation Values: Hydrogen to Lawrencium, Tech. Rep. LA-3691 (Los Alamos Scientific Laboratory, 1968).
- [103] K. B. Nielsen, B. B. Nielsen, J. Hansen, E. Andersen, and J. U. Andersen, Physical Review B 60, 1716 (1999).
- [104] C. H. Seager and R. A. Anderson, Applied Physics Letters 59, 585 (1991).
- [105] T. Zundel and J. Weber, Physical Review B 43, 4361 (1991).
- [106] F. A. Stevie, C. Zhou, M. Hopstaken, M. Saccomanno, Z. Zhang, and A. Turansky, Journal of Vacuum Science & Technology B 34, 03H103 (2016).
- [107] A. M. Stoneham, Theory of Defects in Solids: Electronic Structure of Defects in Insulators and Semiconductors (Oxford University Press, New York, 2001).
- [108] B. Hourahine, R. Jones, S. Öberg, and P. R. Briddon, Materials Science Forum 258-263, 277 (1997).
- [109] J. D. Holbech, B. B. Nielsen, R. Jones, P. Sitch, and S. Öberg, Physical Review Letters 71, 875 (1993).
- [110] V. P. Markevich, L. I. Murin, J. Hermansson, M. Kleverman, J. L. Lindström, N. Fukata, and M. Suezawa, Physica B: Condensed Matter 302-303, 220 (2001).
- [111] P. Leary, R. Jones, and S. Öberg, Physical Review B **57**, 3887 (1998).
- [112] J. L. McAfee and S. K. Estreicher, Physica B: Condensed Matter 340-342, 637 (2003).
- [113] B. Hourahine, R. Jones, S. Öberg, P. R. Briddon, V. P. Markevich, R. C. Newman, J. Hermansson, M. Kleverman, J. L. Lindström, L. I. Murin, N. Fukata, and M. Suezawa, Physica B: Condensed Matter 308-310, 197 (2001).
- [114] C. Peng, H. Zhang, M. Stavola, V. Yelundur, A. Rohatgi, L. Carnel, M. Seacrist, and J. Kalejs, Journal of Applied Physics 109, 053517 (2011).
- [115] T. O. A. Fattah, V. P. Markevich, D. Gomes, J. Coutinho, N. V. Abrosimov, I. D. Hawkins, M. P. Halsall, and A. R. Peaker, Solar Energy Materials and Solar Cells 259, 112447 (2023).
- [116] W. J. Hehre, L. Radom, P. von R. Schleyer, and J. Pople, Ab-Initio Molecular Orbital Theory (Wiley, New York, 1986).
- [117] J. P. Merrick, D. Moran, and L. Radom, The Journal of Physical Chemistry A 111, 11683 (2007).
- [118] B. B. Nielsen, L. Hoffmann, M. Budde, R. Jones, J. P. Goss, and S. Öberg, Materials Science Forum 196-201, 933 (1995).
- [119] M. Budde, G. Lüpke, C. P. Cheney, N. H. Tolk, and L. C. Feldman, Physical Review Letters 85, 1452 (2000).
- [120] M. Budde, C. P. Cheney, G. Lüpke, N. H. Tolk, and L. C. Feldman, Physical Review B 63, 195203 (2001).
- [121] J. M. Pruneda, S. K. Estreicher, J. Junquera, J. Ferrer, and P. Ordejón, Physical Review B 65, 075210 (2002).
- [122] C. Freysoldt, B. Grabowski, T. Hickel, J. Neugebauer, G. Kresse, A. Janotti, and C. G. V. de Walle, Reviews of Modern Physics 86, 253 (2014).
- [123] N. Fukata, S. Fukuda, S. Sato, K. Ishioka, M. Kitajima, T. Hishita, and K. Murakami, Physical Review B 72, 245209

(2005).

- [124] B. Pajot, A. Chari, M. Aucouturier, M. Astier, and A. Chantre, Solid State Communications 67, 855 (1988).
- [125] G. D. Watkins, W. B. Fowler, M. Stavola, G. G. DeLeo, D. M. Kozuch, S. J. Pearton, and J. Lopata, Physical Review Letters 64, 467 (1990).
- [126] S. Wang, ACS Omega 4, 9271 (2019).
- [127] M. Yoneta, Y. Kamiura, and F. Hashimoto, Journal of Applied Physics 70, 1295 (1991).
- [128] R. Kubo, *Statistical Mechanics*, seventh edition ed. (North-Holland, Amsterdam, 1988) pag. 31.
- [129] M. A. Green, Journal of Applied Physics 67, 2944 (1990).